Reciprocal sharing of two classes of public goods facilitates *Bacillus subtilis* biofilm formation

Thibault Rosazza[1], Chris Earl[1], Lukas Eigentler[1,2,3], Fordyce Davidson[2], Nicola R Stanley-Wall[1]

1 Division of Molecular Microbiology, School of Life Sciences, University of Dundee, DD1 4HN Dundee, United Kingdom

2 Mathematics, School of Science and Engineering, University of Dundee, DD1 4HN Dundee, United Kingdom

3 Current address: Evolutionary Biology Department, Universität Bielefeld, Konsequenz 45, 33615 Bielefeld, Germany

Corresponding authors: n.r.stanleywall@dundee.ac.uk
f.a.davidson@dundee.ac.uk

Running title: Public good role of *B. subtilis* extracellular proteases in biofilms

Keywords: *Bacillus subtilis*, extracellular protease, biofilm, public good, reciprocal sharing

Competing interest statement: The authors declare no potential competing interests.

Summary

Public goods support the development of microbial communities but are prone to exploitation. The extracellular matrix molecules of *Bacillus subtilis* are examples of public goods that are produced through the division of labour and support biofilm formation. Another class of public good that supports *B. subtilis* growth when nutrients are in a polymeric form are extracellular proteases. In this study, we investigated the role of extracellular proteases during *B. subtilis* biofilm formation. We established that the extracellular proteases support biofilm growth even when the nitrogen source is available as glutamic acid. Reviewing the contribution played by each protease identified that selected individual extracellular proteases have distinct functions, with AprE found to be crucial for development and WprA sufficient for biofilm formation. We found that changing the nutrient source affected biofilm structure, hydrophobicity, and architecture, likely due to the increased cost of protease dependency for growth. Co-culture of biofilm matrix and extracellular protease mutants rescued biofilm structure through public goods sharing, but the dependence on extracellular protease for growth influenced community coexistence. The intricate sharing among these two classes of public goods sheds light on microbial social dynamics during biofilm formation in different ecological contexts.

Introduction

To persist in diverse environmental contexts, bacteria can deploy various survival strategies, encompassing resistance to specific abiotic conditions, such as nutrient limitation (Harder and Dijkhuizen, 1983), extreme pressure (Merino et al., 2019), or elevated salinity (Oren, 2008). The survival strategies also encompass interactions with biotic factors, including competitive dynamics, such as toxin secretion to impede the growth of neighbouring cells (Hibbing et al., 2010), or mutually beneficial collaborations, such as the division of labour with specific partners allowing coexistence with neighbouring species (West and Cooper, 2016).

In their native habitats, bacteria frequently form sessile, self-encased communities known as “biofilms” (Flemming et al., 2016). Within this context, a mechanism employed by bacteria to secure nutrients involves the synthesis and release of degradative enzymes that selectively target substrates, facilitating the breakdown of complex nutrient sources within their immediate surroundings (Hill et al., 2010, Armstrong, 2015, Cezairliyan and Ausubel, 2017). Illustrating this concept are chitinases, enzymes that break down chitin, a polymer composed of extended chains of N-acetylglucosamine (Hamid et al., 2013). Chitin is ubiquitous in various ecological systems, forming a structural component of fungal cell walls (Schonbichler et al., 2020) and serving as a fundamental element of insects and crustacean exoskeletons (Triunfo et al., 2022). The action of chitinases released by bacteria, such as those produced and secreted by *Vibrio cholerae*, enables the growth and the formation of cell clusters, as the resultant breakdown products serve as a carbon source (Drescher et al., 2014). The chitinases are a public good, as the digested chitin is available for all cells in the surrounding area, whether or not they contribute to the production of the enzymes (Drescher et al., 2014). Strategies, such as biofilm matrix hypersecretion leading to thick biofilms that retain enzymes locally (Drescher et al., 2014), have evolved to reduce sharing with non-producing cells thereby avoiding the so-called tragedy of the commons where the population collapses (Drescher et al., 2014).

Bacillus subtilis, a Gram-positive bacterium, has been the focus of extensive investigation with respect to its ability to form robust, architecturally complex biofilms (Arnaouteli et al., 2021). The capacity of *B. subtilis* to develop biofilms has

widespread ecological and industrial implications ranging from promoting plant health to healing fissures in concrete (Mahapatra et al., 2022, Mahmood et al., 2022). The transition from a free-swimming, planktonic state to a sessile, biofilm-associated mode of growth is governed by a complex network of genetic and environmental factors (Arnaouteli et al., 2021). Residents in the biofilm become encased in a self-produced extracellular matrix, which is primarily composed of polysaccharides, proteins, and nucleic acids (Flemming and Wingender, 2010). In the case of *B. subtilis*, the main biofilm matrix components include fibres of TasA (Branda et al., 2006), an exopolysaccharide (EPS) (Branda et al., 2001), a film-forming protein called BslA (Kobayashi, 2007), and for some conditions and isolates, polyglutamic acid (Morris et al., 2022, Kalamara et al., 2021). These molecules allow the attachment of *B. subtilis* to a surface (Flemming et al., 2007), allow the cells to adhere together (Branda et al., 2006), and provide other important biological functions including the formation of a hydrophobic layer on the surface of the biofilm (Kobayashi, 2007) to name but a few roles that are essential to support biofilm formation and promote the resilience of the resident cells.

B. subtilis has embedded regulatory mechanisms that drive the division of labour and the production of public goods to maximise biofilm productivity (Kearns, 2008, Dragos et al., 2018, Martin et al., 2020). A well-documented example of essential biofilm public goods is the extracellular matrix protein TasA and the EPS (Dragos et al., 2018). The co-culture of TasA and EPS monoproducer strains increases *B. subtilis* ability to form a biofilm at the air-liquid interface. This division of labour arises from the genetic specialisation generating phenotypic heterogeneity within *B. subtilis* biofilm (Lopez et al., 2010). It is also known that during biofilm formation, extracellular proteases are heterogeneously produced within the population (Marlow et al., 2014) and that the suite of eight secreted extracellular proteases is needed to form a wild-type-like colony biofilm, even when glutamic acid serves as the nitrogen source (Earl et al., 2020). It has not been shown if the extracellular proteases function as a public good within biofilms, although, in planktonic conditions, the suite of extracellular proteases serves as a public good that incurs a context-dependent cost that increases as the dependence on the extracellular protease activity for growth rises (Rosazza et al., 2023b).

Here we explore the extent to which the extracellular proteases play a role in supporting biofilm formation by *B. subtilis*. We proposed that the extracellular

110 proteases were a biofilm public good and that the extracellular proteases and matrix
111 molecules could be shared for the mutual benefit of genetically defined non-producer
112 strains during *B. subtilis* biofilm formation. We found that the extracellular proteases
113 and matrix components could be shared, but as the dependency on the extracellular
114 proteases to sustain growth increased, the ability of the genetically defined non-
115 producer strains to coexist in harmony was impacted.

Materials and Methods

Strains and Growth media used in this study

Strains used in this study were derived from *B. subtilis* isolate NCIB 3610 or NCIB 3610 *comIQ12L* (referred to as WT and stocked here as NRS6017) (Konkol et al., 2013) or NCIB 3610 *comIQ12L ΔaprE, Δbpr, Δepr, Δmpr, ΔnprB, ΔnprE, Δvpr, ΔwprA* (referred to as Δ8 and stocked here as NRS5645) (Earl et al., 2019). See Table 1 for a full list. *B. subtilis* strains were routinely grown using Lysogeny-Broth (LB) medium (10 g NaCl, 5 g yeast extract, and 10 g tryptone per litre) at 37°C for 16 hours. For colony biofilm formation, *B. subtilis* strains were grown using an MS base medium (5 mM potassium phosphate and 100 mM MOPS at pH 7.0 supplemented with 2 mM $MgCl_2$, 700 μM $CaCl_2$, 50 μM $MnCl_2$, 50 μM $FeCl_3$, 1 μM $ZnCl_2$, 2 μM thiamine) containing 0.5% (v/v) glycerol (abbreviated to Gly) and one of 0.5% (w/v) glutamic acid (abbreviated to Ga), 1% (w/v) BSA or 1.5% (w/v) milk as required and indicated. Where needed, the medium was solidified using 1.5% (w/v) Select Agar (Invitrogen). The growth medium containing glycerol and glutamic acid is frequently referred to as “MSgg” (Branda et al., 2001).

Growing and imaging colony biofilms

Material from a -80°C glycerol stock was streaked onto an LB plate and incubated O/N at 30°C. A single colony was used to inoculate 5 mL of LB and incubated O/N at 200 rpm at 37°C. 100 μL of the O/N culture was added to 5 mL of LB and incubated at 200 rpm at 37°C. After 4 h, the culture was centrifuged for 10 min at 4500 rpm. The cell pellet was resuspended using 1 mL of base MS media (5 mM K_2HPO_4, 5 mM KH_2PO_4, 100 mM MOPS pH 7.0) and OD_{600} was measured. The culture density was normalised to an OD_{600} of 1 by adding base MS media as required. 10 μL was spotted to establish the colony biofilm. For the co-culture biofilms, the individual isolates were grown as described and mixed in 1 ml at a 1:1 ratio. 10μL of this mixed culture was used to establish the biofilm. The plates were incubated at 30˚C for 1, 2, 3, 6 or 9 days. Depending on the type of experiment performed, biofilms were either imaged using a Nikon camera or a Leica M165C stereoscope or processed to measure biofilm hydrophobicity or extract their protein content. A separate plate was used for each biological replicates and for each time point. Images were uploaded and analysed using the OMERO service or the FIJI software.

148 **Measuring biofilm hydrophobicity**

149 Biofilm hydrophobicity was analysed after 3 days of incubation at 30˚C when the
150 nitrogen source was either glutamic acid or milk and after 6 days for BSA as
151 described previously (Hobley et al., 2013, Kalamara et al., 2021). A contact angle
152 above 90º indicates that the biofilm is non-wetting and a contact angle value below
153 90º indicates that the biofilm is wetting.

154 **Quantifying biofilm footprint area**

155 The footprint occupied by the colony biofilms was quantified using a Python script
156 using the Scikit-image plugin (van der Walt et al., 2014). Images obtained from the
157 Nikon camera (.JPEG files) or the Leica M165C stereoscope (.LIF files) were
158 imported into Python via the pillow or the read LIF plugin. In brief, the biofilm images
159 were cropped and centred to retain biofilm and the border of the Petri dish. A multi-
160 Otsu threshold was calculated to remove background and noise. The biofilm contour
161 was determined using a "marching squares" method (Lorensen and Cline, 1987) to
162 find iso-valued contours in a 2D array and the scale fixed using a reference to yield
163 the area in cm^2.

164 **Quantifying the proportion of a fluorescent population within a colony biofilm**

165 To quantify the proportion of each fluorescent population inside the biofilm footprint
166 area, we used a FIJI macro (Eigentler et al., 2021). The macro consists of defining
167 the biofilm footprint, either automatically or manually, from a dataset of images
168 obtained from the Leica M165C stereoscope (.LIF files). Once assigned, the
169 fluorescent signal intensity is quantified. The relative density of each population is
170 calculated based on amount of pixel values above the background signal (which is
171 the signal in the other fluorescent protein channel) + 2 SD.

172 **Protein extraction and Immunoblotting**

173 For samples grown using glutamic acid 0.5% (w/v) or milk 1.5% (w/v) proteins were
174 extracted after 3 days of incubation at 30˚C. For samples grown using BSA 1% (w/v)
175 proteins were extracted after 6 days of incubation at 30˚C. A tablet of protease
176 inhibitor (Roche) was dissolved into 5 mL of BugBuster protein extraction reagent
177 (Sigma). Using a sterile loop, biofilms were gently recovered and then resuspended
178 into an Eppendorf tube containing 0.5 mL of protease inhibitor BugBuster solution.

179 Biofilms were disrupted by passing through a 23G needle fitted on a 1 mL syringe 5
180 times and then sonicated for 5 sec (2 times) at 30% amplitude with 10 sec intervals
181 ("off time"). Tubes were incubated for 20 min at 21˚C and then centrifuged for 10 min
182 at 13 000 g at 4˚C. A volume of 400 µL of supernatant was transferred into a new
183 Eppendorf tube and protein extracts were stored at -20˚C. To determine the
184 concentration of protein a BCA assay kit was used (Pierce).

185 10 µg of protein mixed with 7.5 µL of 4X loading dye (0.5 M Tris-HCl pH 6.8, 0.1 M
186 EDTA, 15.5% (w/v) SDS, 3% (v/v) glycerol, 5% (v/v) β-mercaptoethanol, 1 mg
187 bromophenol blue) and H_2O was added to bring the total volume to 30 µL. To
188 denature proteins, tubes were incubated for 5 min at 95˚C and centrifuged 1 min at
189 13 000 rpm. 30 µL samples were loaded onto a 10% (w/v) SDS-PAGE gel and run
190 for ±1 h at 120 volts prior to transfer to a polyvinylidene difluoride membrane. The
191 membrane was transferred to a 50 mL Falcon tube and washed using 1x TBS
192 containing Tween 0.2% (v/v) and then incubated at 4˚C on a roller shaker for 1 h in 5
193 mL of TBS Tween 0.2% (v/v) + milk 3% (w/v) solution. The membranes were washed
194 and incubated O/N at 4˚C on a roller shaker in 5 mL of TBS Tween 0.2% (v/v) + milk
195 3% (w/v) solution containing the primary antibody. For αBslA (rabbit) a 1:500 dilution
196 was used and αTasA (rabbit) a 1:25000 dilution was used (Ostrowski et al., 2011).
197 Membranes were transferred into a new 50 mL Falcon tube and washed as
198 described above prior to incubation in 5 mL of TBS Tween 0.2% (v/v) + milk 3% (w/v)
199 containing αRabbit-HRP (goat) secondary antibody at a 1:5000 dilution. The
200 membranes were washed as above and a mix of 1 mL ECL1 and 1 mL ECL2
201 solution (Thermo Fisher) used for signal detection via an Azure scanner. Images
202 were visualised using FIJI software.

203 **Determining biofilm productivity and sporulation percentage**

204 After 3 days of incubation at 30˚C, biofilms were transferred from the agar surface
205 into 1mL of PBS 1X using a sterile loop. The biomass was disrupted by multiple
206 passage through a 23G needle and sonication for 3 sec (2 times) at 20% amplitude
207 with 10 sec intervals ("off time"). To determine the number of CFU/biofilm, 10-fold
208 serial dilutions were performed up to 10^{-8} in 1 mL of PBS 1X and 100 µL of the 10^{-8}
209 dilution was plated onto the surface of an LB agar plate. To determine the proportion
210 of spores per biofilm, the remaining 900 µL of the 10^{-8} dilution was heat-treated for

211 20 min at 80˚C and left to cool for 10 min at room temperature. 100 µL of this heat-
212 treated sample was plated onto LB agar plate after mixing. The agar plates were
213 incubated O/N at 37˚C and the number of CFUs on each plate was enumerated to
214 calculate the CFU/biofilm and CFU spores/biofilm.

215 **Data analysis and visualisation**

216 To analyse and visualise datasets acquired we used Python scripts and plugins.
217 Jupyter notebook (Kluyver et al., 2016) was used to import, clean, and analyse all
218 the datasets. Matplolib (Hunter, 2007) and Seaborn (Waskom, 2021) plugins were
219 used to visualise and export graphs obtained from the datasets analysis. Stats plugin
220 was used to perform all statistical analysis. T-tests were performed to compare the
221 mean of each relevant condition at different timepoints. P-values from comparison
222 between NCIB 3610 and other relevant strains at different timepoints were included
223 in the figures (*** = p-value<0.001, ** = p-value<0.01, *= p-value<0.05). The datasets
224 and code generated are available in a Zenodo repository (Rosazza et al., 2023a).

225

Results

The extracellular proteases are needed for wild-type colony biofilm formation. NCIB 3610 (a wild-type (WT) protease-producing isolate) forms a rugose colony biofilm when glutamic acid is the main nitrogen source (Figure 1A, 1B) (Branda et al., 2001). In the same conditions, the Δ8 strain (NRS5645 - a derivative of NCIB 3610 that lacks the coding regions of the eight known extracellular proteases (Earl et al., 2020)) forms an expanded colony biofilm where the interior lacks wrinkles and the periphery develops limited wrinkles after 3-days of incubation (Figure 1A, 1B). Quantification of the surface area occupied by the colony biofilms revealed a larger footprint for the Δ8 strain compared to the protease-producing parental strain at all time points from 48 hours onwards (Figure 1C). These results confirm and extend our previous work (Earl et al., 2020), demonstrating that when nitrogen is in the form of glutamic acid, the extracellular proteases support biofilm architecture development and restrict biofilm expansion.

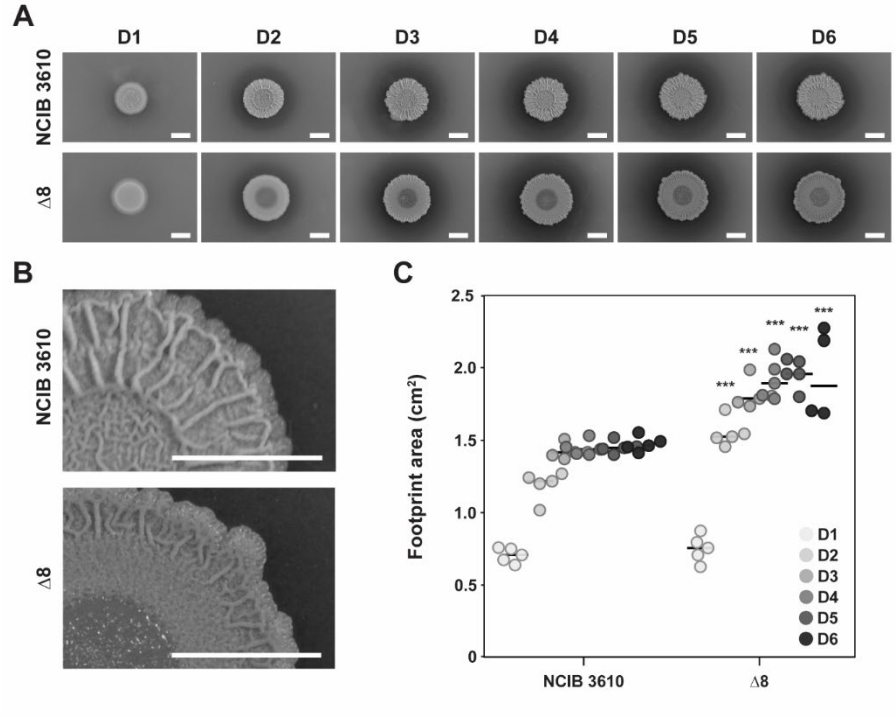

Figure 1 - Extracellular proteases support formation of rugose colony biofilm. A. Images of NCIB 3610 and Δ8 strains over time (day 1 to day 6, D1-D6) grown using MS base supplemented with 0.5% glutamic acid (w/v). A representative image of five independent experiments is shown; **B.** Close-up of NCIB 3610 and Δ8 biofilms at D6 from Figure 1A. The scale bar represents 5 mm; **C.** Biofilm footprint area in cm^2 of NCIB 3610 and Δ8 strains over time (day 1 to day 6) grown using 0.5% glutamic acid (w/v). Each point represents the footprint area value (n=5 biological replicates) and the line represents the median value. T-test were

249 performed between NCIB 3610 and Δ8 strain at each time point: *** = p-value <
250 0.001.

251

252 **The impact of specific extracellular proteases on colony biofilm formation.**
253 We predicted that there would be redundancy in the extracellular proteases required
254 to achieve wild-type colony biofilm formation, meaning that deletion of any single
255 gene encoding an extracellular protease would be likely to have a limited impact on
256 the colony biofilm phenotype. To explore this hypothesis, we used a suite of single
257 extracellular protease mutant strains (see Table 1) (Rosazza et al., 2023b). We
258 spotted colony biofilms for each deletion strain and imaged their formation over 3
259 days, a time frame where the phenotypic difference between NCIB 3610 and Δ8 is
260 striking. We found that when *B. subtilis* was engineered not to produce one of Bpr,
261 Epr, Mpr, NprB, NprE, Vpr or WprA there was no impact on the colony biofilm
262 phenotype, with each single deletion strain exhibiting a NCIB 3610-like phenotype
263 (Figure S1A). The finding for Vpr was consistent with our previous results (Earl et al.,
264 2020) and that of others for NprB (Kobayashi and Ikemoto, 2019). In contrast, not
265 producing AprE affected the formation of wrinkles (Figure 2A, 2B). The *aprE* mutant
266 colony biofilms were less structured, and the wrinkles were less abundant and
267 prominent than those observed on NCIB 3610 biofilms. The phenotype of the *aprE*
268 single mutant colony biofilm was different from the Δ8 strain with small wrinkles
269 being placed across the entirety of the biofilm surface for the *aprE* mutant strain
270 rather than solely at the extremity. We found that the *wprA* mutant footprint was
271 comparable to the NCIB 3610 parental strain (Figure S1B). The *epr* mutant had a
272 biofilm footprint area that fell between the NCIB 3610 and Δ8 strain (Figure S1B),
273 while the remaining single deletion mutants had a similar biofilm footprint area to that
274 of the Δ8 strain (Figure S1B).

275

276 To isolate the role of each extracellular protease and examine its role in supporting
277 colony biofilm formation, we repeated the analysis using a library of extracellular
278 protease mono-producer strains (where a single coding region was reinserted into
279 the Δ8 strain (Table 1) (Rosazza et al., 2023b)). We observed that only the WprA
280 mono-producer strain had a wrinkle phenotype that was comparable to NCIB 3610
281 (Figure 2C, 2D). The Mpr mono-producer strain had a phenotype that was
282 intermediate to that of the WT producer strain and the Δ8 strain (Figure 2C, 2D). All

283 the other mono-producer strains only displayed wrinkles at the edge of the biofilm
284 like the Δ8 strain (Figure S1B). Quantification of the biofilm footprint area of these
285 strains revealed that producing one of Bpr, Epr, Mpr and WprA increased the ability
286 of *B. subtilis* to expand during biofilm formation (Figure 2E), with the footprint
287 occupied increasing beyond that attained by the Δ8 strain. By contrast, restoration of
288 Vpr production to the Δ8 strain impeded the ability of the isolate to expand such that
289 the colony biofilm footprint of the *vpr* monoproducer strain was the same as the WT
290 (Figure 2E). The reintroduction of *aprE* or *nrpB* or *nprE* had no impact on the colony
291 biofilm footprint occupied compared with the Δ8 strain (Figure 2E).
292
293 Taken together, these results allowed us to identify that the removal of AprE from the
294 NCIB 3610 secretome has a negative impact on colony biofilm architecture and
295 WprA activity (where production is driven by its native promoter) alone is sufficient to
296 promote wrinkle development within the colony biofilm. Moreover, altering the profile
297 of extracellular proteases produced impacts the ability of *B. subtilis* to expand during
298 biofilm formation in a protease-specific manner and a manner that is independent of
299 the ability of the strain to form rugose colony biofilms.

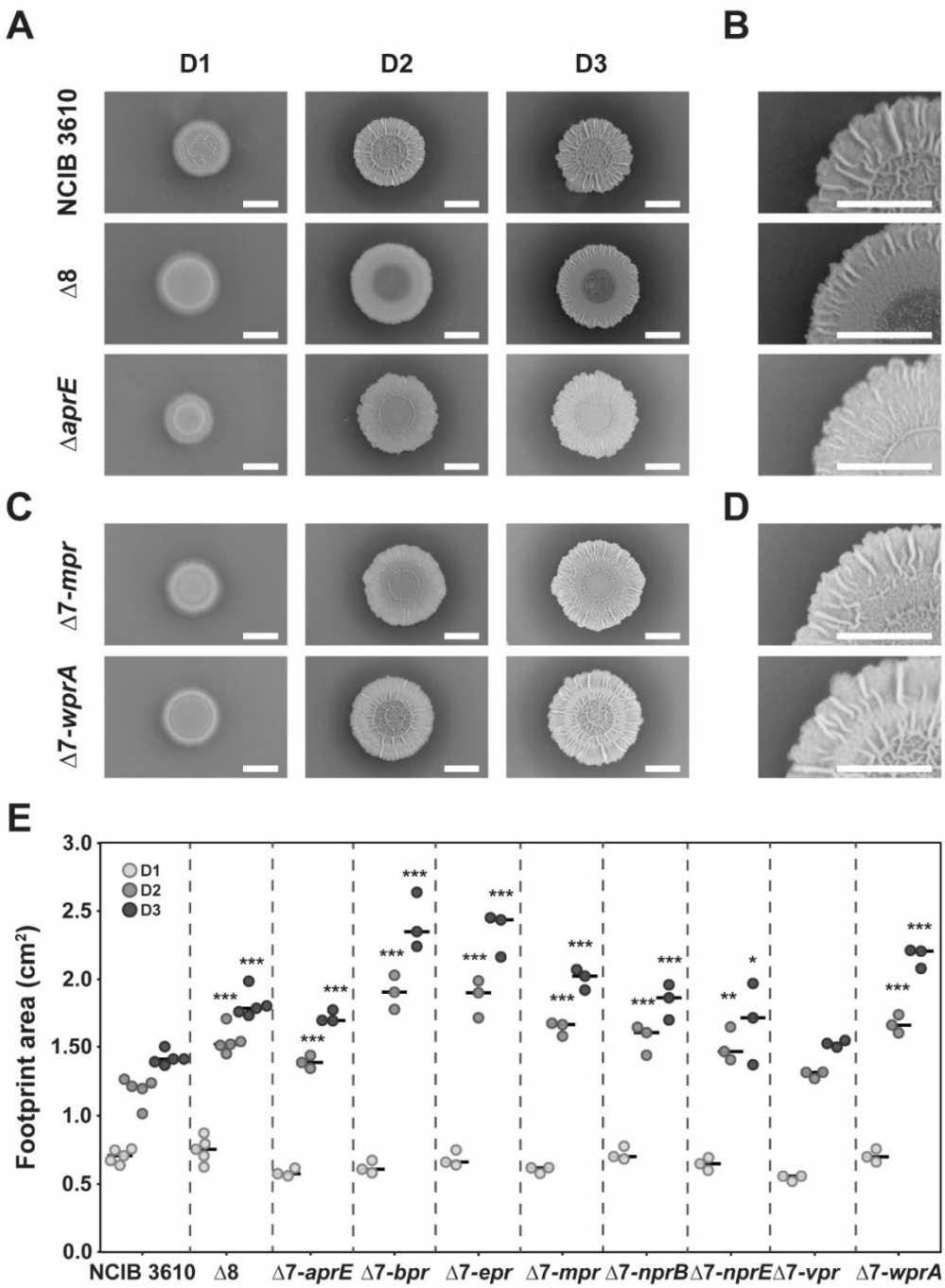

Figure 2 – Specific extracellular proteases support the formation of a wrinkled colony biofilm. **A.** Images of NCIB 3610, Δ8 and Δ*aprE* colony biofilms over time (day 1 to day 3); **B.** Close-up of NCIB 3610, Δ8 and Δ*aprE* biofilms at D3 from Figure 2A.; **C.** Images of NCIB 3610, Δ8, Δ7-*mpr* and Δ7-wprA colony biofilms over time (day 1 to day 3); **D.** Close-up of NCIB 3610, Δ8, Δ7-*mpr* and Δ7-wprA biofilms at D3 from Figure 2C; **E.** Biofilm footprint area in cm^2 of NCIB 3610, Δ8, Δ7-*aprE,* Δ7-*bpr,* Δ7-*epr,* Δ7-*mpr*, Δ7-*nprB,* Δ7-*nprE,* Δ7-*vpr* and Δ7-*wprA* strains over time (day 1 to day 3) in. Each point represents the footprint area value (n=5 biological replicates) and the line represents the median value. A representative image of five independent experiments is shown. T-test performed between NCIB 3610 and Δ8 strains or monoproducer strains (see Table 1) at each time point: *** = p-value <

0.001, ** = p-value < 0.01, * = p-value < 0.05. All scale bars represent 5 mm. All samples were grown using 0.5% glutamic acid (w/v) and 0.5% glycerol (v/v).

The proteinaceous extracellular matrix components are produced in the absence of the extracellular proteases.

We hypothesized that the Δ8 strain colony biofilm defect may be a consequence of lacking one of the proteinaceous extracellular matrix components (namely BslA (Kobayashi, 2007) and/or TasA (Branda et al., 2006)). We assessed the ability of the Δ8 strain to produce BslA and TasA using a triple extracellular matrix component mutant strain (Δ*bslA*, Δ*eps(A-O)*, Δ*tasA* (ΔbΔeΔts) NRS6552) as a negative control for the immunoblot analysis. We grew colony biofilms for three days (Figure 3A) and extracted proteins from the entire biomass. Neither TasA nor BslA were detected in the negative control sample (Figure 3B). We detected both BslA and TasA proteins in the Δ8 biofilm samples (Figure 3B). However, in the NCIB 3610 protein extract, the TasA protein was present at its native molecular weight (~28 kDa) and at a lower molecular weight (~10 kDa). In the Δ8 biofilm protein extract, the TasA protein was only present at its apparent native molecular weight (~28 kDa). These results indicate that the two main extracellular matrix proteins are produced independently of extracellular protease activity. However, not producing the extracellular proteases impedes the extracellular protease-dependent cleavage of TasA. We currently do not know if the lack of TasA cleavage in the Δ8 strain is responsible for the impact observed on colony biofilm formation.

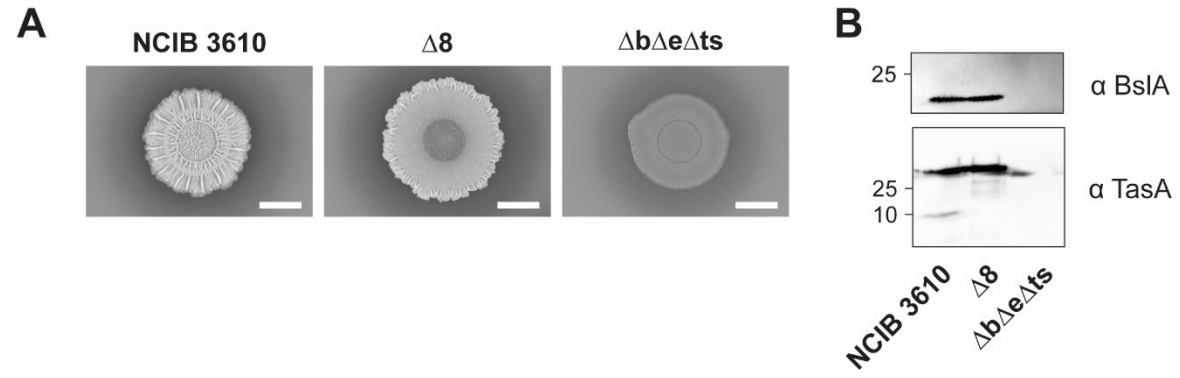

Figure 3 - Extracellular matrix proteins are produced in the absence of extracellular proteases. A. Images of NCIB 3610, Δ8 and Δ*bslA*, Δ*eps(A-O)*, Δ*tasA* (ΔbΔeΔts) colony biofilms at day 3. A representative image of five independent experiments is shown. The scale bar represents 5 mm; **B.** Immunoblot analysis of BslA (top image) and TasA (bottom image) in biofilm protein extracts obtained after 3 days from NCIB 3610, Δ8 (NRS5645) and Δ*bslA*, Δ*eps(A-O)*, Δ*tasA* (NRS6552)

341 (labelled ΔbΔeΔts) colony biofilms. A representative image of three independent
342 experiments is shown for the colony biofilms. All samples were grown using 0.5%
343 glutamic acid (w/v) and 0.5% glycerol (v/v). The scale bar represents 5 mm.

344 **The absence of extracellular proteases increases sporulation**

345 We next tested if the phenotypic difference observed between NCIB 3610 and Δ8
346 strains during biofilm formation was due to a growth difference that emerged under
347 sessile conditions. This proposition was founded on the knowledge that biofilm
348 wrinkle formation is associated with the spatial constraints imposed during biofilm
349 formation that physically force the cells to grow on top of one another (Asally et al.,
350 2012, Fei et al., 2020) and that cells lyse, presumably releasing complex molecules
351 into the biomass (Asally et al., 2012). As a measure of growth, and thus biofilm
352 productivity, we quantified the number of CFUs per biofilm for the NCIB 3610, Δ8,
353 and Δ*bslA* Δ*eps(A-O)* Δ*tasA* strains. The colony biofilm formed by the Δ*bslA* Δ*eps(A-*
354 *O)* Δ*tasA* strain contained approx. 700-fold fewer CFU/biofilm compared to the WT
355 strain (Figure 4A), confirming previous results showing that not producing biofilm
356 matrix proteins impacts biofilm productivity (Dragos et al., 2018). The difference in
357 biofilm productivity in terms of the number of CFU/biofilm quantified between the
358 NCIB 3610 and the Δ8 strain was marginal with approx. 1.6-fold higher in the Δ8
359 strain (Figure 4A).
360

361 *B. subtilis* can form spores when nutrients are limited (Errington, 1993). Therefore,
362 we quantified the proportion of spores in the colony biofilms for the same strains.
363 The proportion of spores in Δ*bslA* Δ*eps(A-O)* Δ*tasA* biofilms was lower (about half)
364 than that of the NCIB 3610 biofilm (Figure 4B), confirming that not producing biofilm
365 matrix proteins impedes the ability of the resident cells to sporulate (Vlamakis et al.,
366 2008). By contrast, the proportion of spores was consistently higher in Δ8 colony
367 biofilms than the wild-type strain (Figure 4B) with around 2-fold more spores in the
368 protease-free strain. Thus, not producing extracellular proteases seems to increase
369 the probability of the cells sporulating during biofilm formation, which may be linked
370 with a lack of access to nutrients, especially in the founding part of the colony biofilm
371 that has restricted access to nutrient sources in the surrounding agar or in the
372 polymeric material released from lysed cells. These findings show that by
373 comparison to planktonic conditions (Rosazza et al., 2023b), extracellular proteases

are likely to play a role in supporting and/or sustaining growth in colony biofilm even when a non-polymeric nitrogen source is provided.

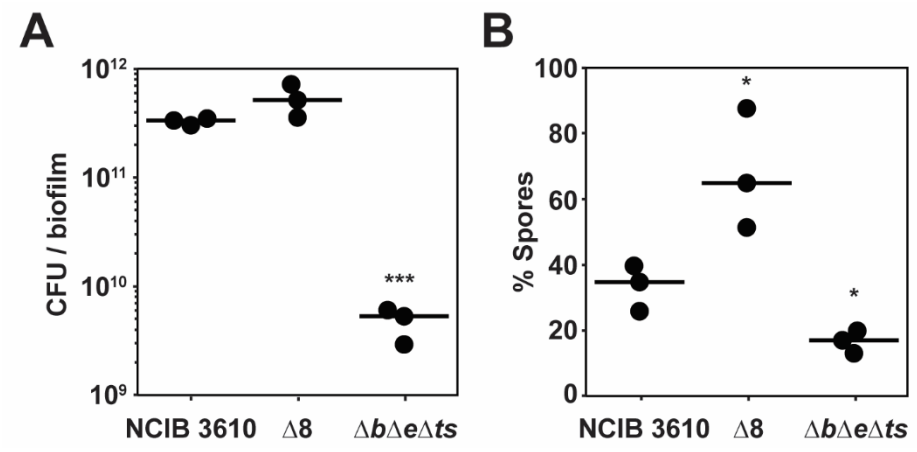

Figure 4 - Biofilm productivity and sporulation are impacted by absence of extracellular proteases. A. Biofilm productivity at day 3 for NCIB 3610, Δ8 and Δ*bslA*, Δ*eps(A-O)*, Δ*tasA* (ΔbΔeΔts) strains. Each point represents the CFU/biofilm (n=3 biological replicates) and the line represents the median value. T-test performed between NCIB 3610 and Δ8 or ΔbΔeΔts strains: *** = p-value < 0.001; **B.** Proportion of spores per biofilm at day 3 for NCIB 3610, Δ8 and Δ*bslA*, Δ*eps(A-O)*, Δ*tasA* (ΔbΔeΔts) strains. Each point represents the % sporulation (n=3 biological replicates) and the line represents the median value. T-test performed between NCIB 3610 and Δ8 or ΔbΔeΔts strains: * = p-value < 0.05. All samples were grown using 0.5% glutamic acid (w/v) and 0.5% glycerol (v/v).

Reciprocal sharing of two classes of public goods recovers *B. subtilis* colony biofilm morphology.

The biofilm matrix and extracellular protease non-producer strains each have impaired colony biofilm formation phenotypes, albeit for different reasons. We explored if reciprocal sharing of the extracellular proteases and the biofilm matrix molecules during co-culture could reinstate an NCIB 3610-like phenotype (Figure 5A). To test this, we spotted a mix at an initial 1:1 ratio of the Δ8 strain expressing mKate with either single matrix mutant (Δ*bslA*, Δ*eps(A-O)* or Δ*tasA*) or a triple matrix mutant (Δ*bslA*, Δ*eps(A-O)*, Δ*tasA*) strain expressing GFP (see Table 1 for strain details). We also performed the co-cultures using NCIB 3610 instead of the Δ8 strain as a reference (Figure S2). We evaluated the ability of the co-cultured strains to form a structured biofilm and assessed if the phenotype was comparable to that of the NCIB 3610 strain grown alone under the same conditions. We assessed the proportion of the two strains at the end of the experiments using image analysis methods (Eigentler et al., 2021) to determine if the ratio had deviated from the initial

403 1:1 founder ratio. Finally, we quantified the footprint occupied by the biomass
404 (Eigentler et al., 2021). A summary of the findings is shown in Table 2.
405
406 We observed that compared to the extracellular protease and extracellular matrix
407 component mutants cultured in isolation (Figure 5A), co-culturing the Δ8 strain with
408 any of the single matrix mutants (Δ*bslA,* Δ*eps(A-O)* or Δ*tasA*) or the triple matrix
409 mutant (Δ*bslA,* Δ*eps(A-O),* Δ*tasA*) strain largely restored NCIB 3610-like colony
410 biofilm formation (Figure 5B). Compared to the flat phenotype of the extracellular
411 matrix component mutant strains, and the situation where only the edge of the
412 colony biofilm displayed wrinkles in the case of the Δ8 strain (Figure 5A), the
413 presence of both mutant strains in the founding community allowed the formation of
414 wrinkles across the biofilm (Figure 5B). The same outcome was observed when we
415 combined the NCIB 3610 strain expressing mKate with any of the single matrix
416 mutant (Δ*bslA,* Δ*eps(A-O)* or Δ*tasA*) or the triple matrix mutant (Δ*bslA,* Δ*eps(A-O),*
417 Δ*tasA*) strains expressing GFP at a 1:1 starting ratio (Figure S2A).
418
419 We quantified the relative density of each population within the mature biofilms using
420 the fluorescent protein reporters and observed that both the Δ8 and NCIB 3610
421 strains coexisted with each type of matrix mutants (Figure 5C and Figure S2B), with
422 the NCBI 3610 or Δ8 strain present at a similar proportion to the matrix mutants at
423 the end of the experiment (Figure 5C and Figure S2B). All strain combinations
424 exhibited a higher biofilm footprint area compared to the NCIB 3610 strain (Figure
425 5D). Taken together, we can conclude that the extracellular proteases and
426 extracellular matrix producer strains coexist during biofilm formation and that the
427 reciprocal sharing of the two types of public goods between the Δ8 and matrix
428 mutant strains can rescue the NCIB 3610-like colony biofilm phenotype but does not
429 prevent increased surface occupancy.

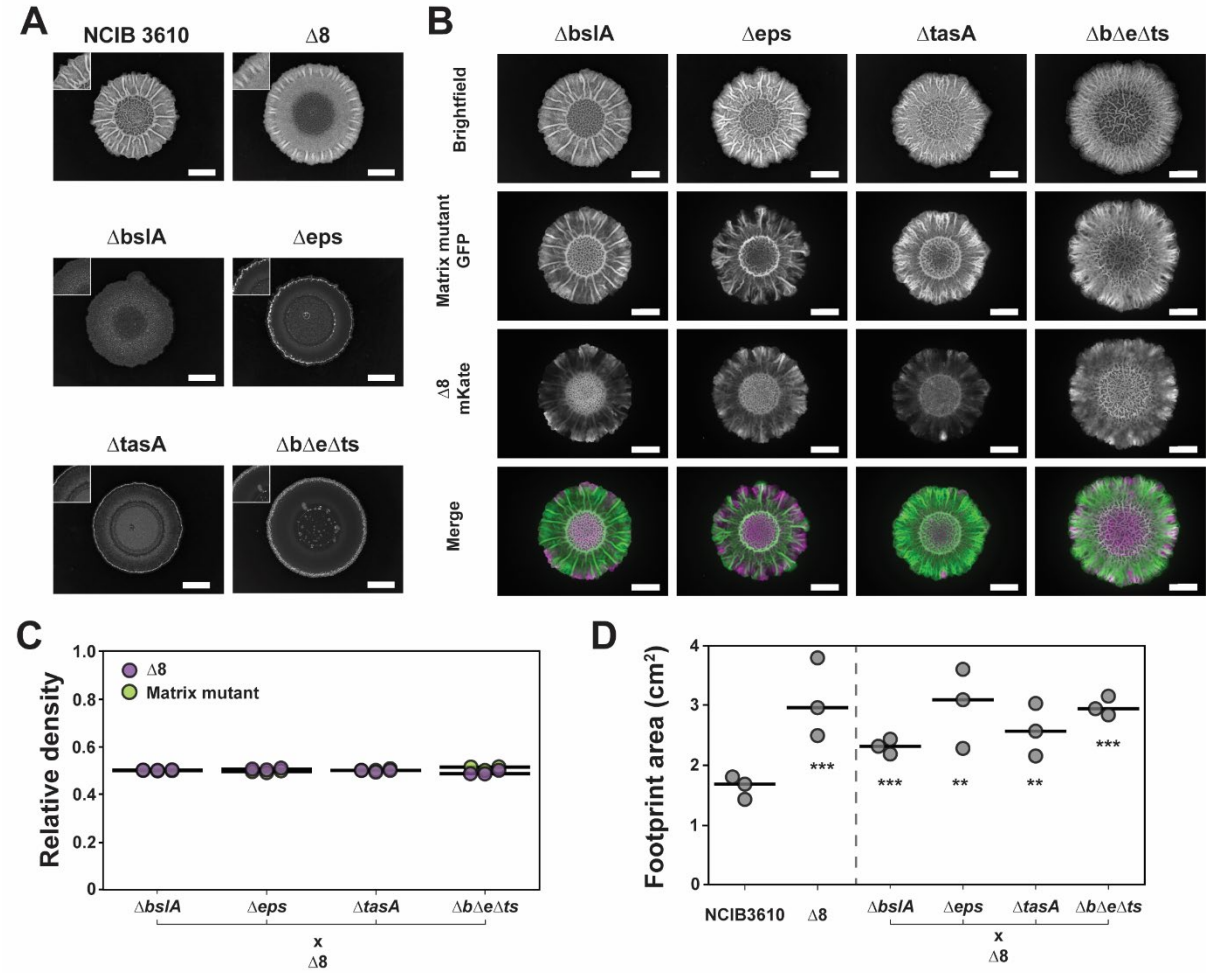

Figure 5 Extracellular proteases and extracellular matrix molecules are biofilm public goods. A. Images of NCIB 3610-mKate, Δ8-mKate, Δ*bslA*-GFP, *Δeps(A-O)*-GFP, Δ*tasA*-GFP and *ΔbslA, Δeps(A-O),ΔtasA* (ΔbΔeΔts) -GFP colony biofilms at day 3. A close-up is shown in the top-right corner.; **B.** Images of colony biofilms founded using a 1:1 ratio of Δ8-mKate:ΔbslA-GFP, Δ8-mKate:Δeps(A-O)-GFP, Δ8-mKate:ΔtasA-GFP, or Δ8-mKate:ΔbslA, Δeps(A-O),ΔtasA (ΔbΔeΔts)-GFP strains at day 3. The raw intensity signal for brightfield, GFP, and mKate proteins is shown in greyscale and the merge intensity signal of these two proteins is false coloured (green=GFP, magenta=mKate); **C.** Quantification of the relative density of the GFP and mKate signal within the biofilm footprint. Each point represents the relative density value (n=3) and the line represents the median value; **D.** Biofilm footprint area in cm^2 of NCIB 3610, Δ8 and the conditions presented in B. Each point represents the footprint area value (n=5 biological replicates) and the line represents the median value. T-test performed between NCIB 3610 and Δ8 or coculture mixes: *** = p-value < 0.001, ** = p-value < 0.01. The scale bar represents 5 mm. A representative image of three independent experiments is shown. Samples were grown using 0.5% glutamic acid (w/v) and 0.5% glycerol (v/v).

The nutrient source influences biofilm structure and hydrophobicity

450 The relative cost associated with extracellular protease production increases as the
451 dependence on their activity for growth rises and the ability of the producer strain to
452 support the growth of non-producers drops (Rosazza et al., 2023b). We aimed to
453 examine the impact of the increasing relative cost of extracellular protease
454 production on biofilm formation, and on the ability of the genetically defined public
455 good non-producing strains to share materials. However, we first needed to identify
456 growth conditions where biofilm formation occurred, but where growth depended
457 more highly on extracellular protease activity. The presence of polymeric nutrient
458 sources forces a dependency on extracellular proteases for growth in planktonic
459 conditions (Rosazza et al., 2023b). Therefore, we replaced the glutamic acid in our
460 growth medium with either 1.5% (w/v) milk or 1% (w/v) bovine serum albumin (BSA)
461 and assessed the ability of NCIB 3610 and the ∆8 strain to form colony biofilms. For
462 the milk-containing medium, rapid growth of a structured biofilm for the NCIB 3610
463 strain was achieved and, while the Δ8 strain managed to grow, albeit to a much
464 lower extent than the NCIB 3610 strain, it did not manage to form a structured biofilm
465 (Figure 6A) and the footprint was significantly smaller (Figure 6B). When 1% BSA
466 (w/v) formed the polymeric source of nitrogen, we detected the formation of a colony
467 biofilm for the NCIB 3610 strain. The colony biofilm showed signs of rugosity, which
468 is indicative of the production of biofilm matrix molecules (Figure S3), albeit to a
469 lower extent than when glutamic acid was used as the nitrogen source (compare
470 with Figure 1B). In the same conditions, growth of the ∆8 strain was significantly
471 impeded (Figure 6A). The biomass that was present on the agar surface occupied a
472 smaller footprint than the protease producing strain (Figure 6B) and showed no
473 evidence of wrinkles (Figure 6A). These observations confirm a dependency on the
474 extracellular proteases for growth as previously measured in planktonic conditions
475 (Rosazza et al., 2023b).
476
477 We assessed the properties of the colony biofilms formed and tested the
478 dependency on the known extracellular matrix molecules to support colony biofilm
479 structure. When the nutrient source was milk, we observed that each matrix mutant
480 strain (Δ*bslA,* Δ*eps,* or Δ*tasA*) had a halo surrounding them where the milk contained
481 in the agar had been degraded (Figure 6D). Thus, the extracellular matrix mutants
482 can produce extracellular proteases. In terms of biofilm morphology, in contrast to

483 glutamic acid mediated growth, the Δ*bslA* strain formed a structured biofilm that was
484 largely comparable to that of the parental strain NCIB 3610 on both milk and BSA-
485 containing growth media. The Δ*eps(A-O)* and Δ*tasA* mutants grew on all these
486 media and, as noted for other conditions and contexts (Dragos et al., 2018), had a
487 defect in forming a structured colony biofilm (Figure 6D).
488
489 As the Δ*bslA* strain formed a WT-like wrinkled biofilm when the nitrogen source was
490 polymeric, we hypothesised that the production of BslA might be repressed in these
491 conditions. BslA is needed for NCIB 3610 colony biofilm hydrophobicity (Kobayashi
492 and Iwano, 2012) and structure (Ostrowski et al., 2011), although the two functions
493 are genetically separable (Arnaouteli et al., 2017). Therefore, we tested if the colony
494 biofilms were hydrophobic and if BslA was produced by the residents. We did not
495 detect any surface hydrophobicity for the NCIB 3610 biofilm on either polymeric
496 nutrient source media. Compared to growth using glutamic acid as the nitrogen
497 source, the contact angle of the water droplet was below 90˚ (indicating a hydrophilic
498 or wetting surface) (Figure 6E). However, when we used immunoblotting to assess
499 protein extracts obtained from the NCIB 3610 biofilm grown using milk or BSA as the
500 polymeric nitrogen source, we were able to detect presence of BslA (Figure 6C). We
501 used TasA as a control, and as we expected, we could detect it in within the WT
502 protein sample in both conditions by immunoblotting, its presence being consistent
503 with the *tasA* mutant strain displaying a colony biofilm defect in these conditions
504 (Figure 6C). As the Δ8 strain was not able to grow well in these conditions, we could
505 not extract protein from the small cell aggregates and could not analyse the material
506 by immunoblot. These results indicate that BslA is produced, but is not required for
507 biofilm structure in these nutrient conditions, consistent with its dispensability for
508 biofilm formation in some conditions, for example on fungal hyphae (Kjeldgaard et
509 al., 2019).

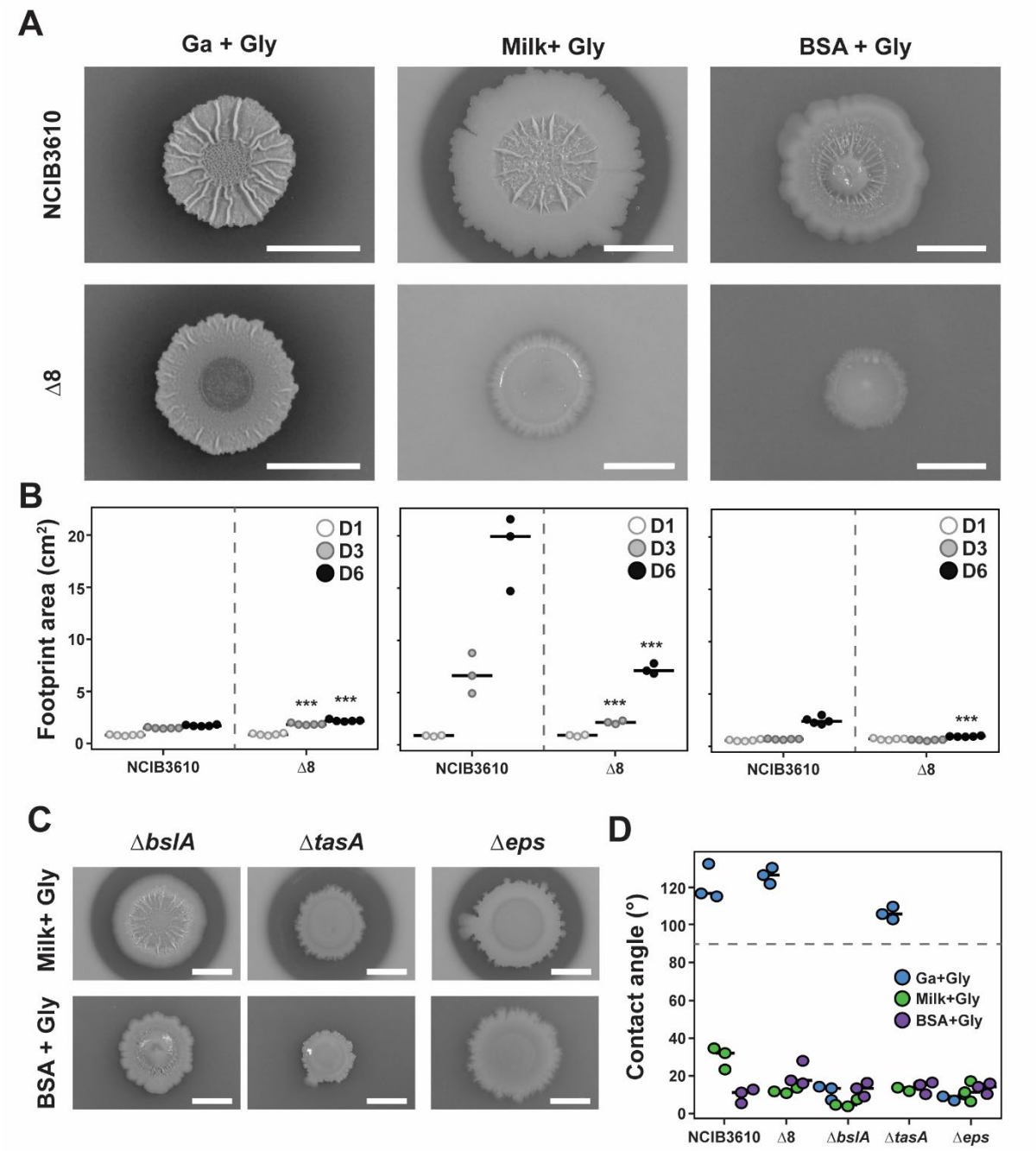

Figure 6 – Food accession change biofilm morphology A. Biofilm reflected light images of NCIB 3610 and Δ8 strains at day 3 (0.5% glutamic acid (Ga) (w/v) and 1.5% milk (w/v)) and day 6 (1% BSA (w/v)). **B.** Biofilm footprint area in cm^2 of NCIB 3610, Δ8 and the conditions presented in A. Each point represents the footprint area value (n=5 biological replicates) and the line represents the median value. T-test performed between NCIB 3610 and Δ8 strain at each time point: *** = p-value < 0.001; **C.** Biofilm reflected light images of ΔbslA , Δeps(A-O) and ΔtasA strains at day 3 (0.5% glutamic acid (Ga) (w/v) and 1.5% milk (w/v)) and day 6 (1% BSA (w/v)). **D.** Contact angle quantification of water droplet on biofilm of NCIB 3610, Δ8 *ΔbslA* , *Δeps(A-O)* and *ΔtasA* strains at day 3 (0.5% glutamic acid (Ga) (w/v) and 1.5% milk (w/v)) and day 6 (1% BSA (w/v)). Each point represents the contact angle values (n=3 biological replicates) and the line represents the median value. In all cases the

523 scale bar represents 5 mm. A representative image of three independent
524 experiments is shown.

525

526 **Reciprocal sharing of public goods restores structured biofilms but impacts**
527 **coexistence when the relative cost of extracellular protease production is high.**

528

529 Having established conditions for *B. subtilis* colony biofilm formation that depend on
530 the two different classes of public goods, we assessed the impact on reciprocal
531 sharing with the matrix mutants. Using the same strategy, we spotted a mix of either
532 NCIB 3610 or Δ8 strains expressing mKate with either a single matrix mutant (Δ*bslA,*
533 Δ*eps(A-O)* or Δ*tasA*) or the triple matrix mutant (Δ*bslA,* Δ*eps(A-O),* Δ*tasA*) strain
534 expressing GFP at a 1:1 ratio. We evaluated the ability of the community to form a
535 structured biofilm and assessed if the structure was comparable to that of the NCIB
536 3610 strain grown under the same conditions. A summary of the findings is shown in
537 Table 2.

538

539 When the nitrogen source was milk, a significant recovery towards the morphology of
540 the NCIB 3610 phenotype on the same conditions was observed when the Δ8 strain
541 was co-cultured with either the *bslA*, *eps(A-O)*, *tasA* single mutant strains or the
542 triple matrix mutant, (Figures 7A, 7B). Broad coexistence of the founding isolates in
543 the mature community was seen, except for the Δ8:*eps(A-O)* mutant combination
544 where the Δ8 strain dominated (Figure 7D). For this strain combination, a reduction
545 in the footprint occupied by the biomass compared to NCIB 3610 was also quantified
546 (Figure 7E). These data show the isolates can share the two classes of public goods
547 but reveal that there is a higher cost associated with the production of the biofilm
548 polysaccharide (as it was outcompeted). Co-culture of the matrix mutant strains with
549 NCBI 3610 in these conditions, broadly revealed the same outcomes but a minor
550 reduction in the footprint occupied when its partner strain lacked the *tasA* coding
551 region (Figures S4A, S4B). These data show the ability of the WT strain to
552 accommodate the non-producing matrix mutant without a significant impact on
553 fitness.

554

555 When the dependence on the extracellular proteases for growth was further
556 increased, which was achieved by replacing milk with BSA the ability of the two

557 founding strains to recover a wild-type-like biofilm morphology and to coexist
558 decreased (Figure 7A, 7C). However, a partial recovery towards the morphology of
559 the NCIB 3610 colony biofilm was observed when the Δ8 strain was co-cultured with
560 one of the *bslA*, *eps(A-O)*, *tasA* single mutant strains or the triple matrix mutant
561 (Figure 7A, 7B). Analysis of the population composition indicated that the Δ8 strain
562 had a competitive advantage when co-cultured with either the *bslA*, *tasA* or triple
563 mutant strains (Figure 7F). In contrast, Δ8 had a lower competitive advantage when
564 mixed with the *eps(A-O)* mutant (Figure 7F). We noted that the biofilm footprint of the
565 Δ8 strain co-cultured with either the *eps(A-O)*, *tasA* or the triple mutant was
566 significantly greater than that of the NCIB 3610 colony biofilm (Figure 7G), indicative
567 of increased productivity in terms of surface area colonisation. Co-culture of the *bslA*,
568 *eps(A-O)* and *tasA* matrix mutant strains with NCBI 3610 broadly revealed the same
569 outcome (Figure S4C, S4D). However, a different impact on biofilm structure was
570 observed when NCIB 3610 was co-cultured with the triple matrix mutant. In this
571 case, the biofilm community exhibited a high degree of spatial segregation between
572 the two isolates, with the triple mutant being more represented in the population and
573 localised at the edge of the biofilm (Figure S4C).

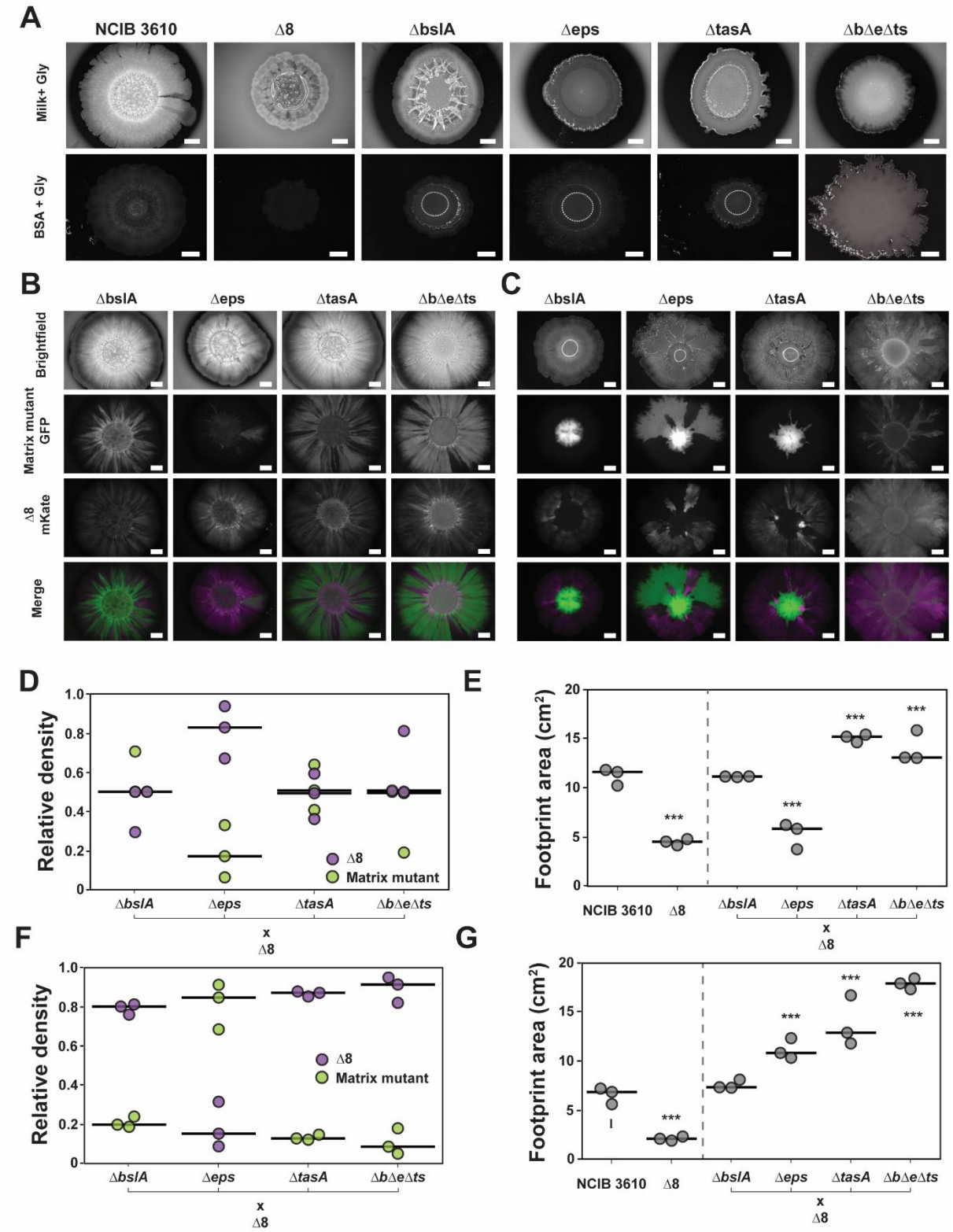

Figure 7 – Extracellular proteases and extracellular matrix component producers engaged differentially in the division of labour in the presence of hard-to-access nutrient sources A. Biofilm stereoscope images of NCIB 3610-mKate, Δ8-mKate, ΔbslA-GFP, Δeps(A-O)-GFP, ΔtasA-GFP and ΔbslA, Δeps(A-O),ΔtasA (ΔbΔeΔts) -GFP strains at day 3 (0.5% glutamic acid (Ga) (w/v) and 1.5% milk (w/v)) and day 6 (1% BSA (w/v)); **B.** Biofilm stereoscope images of a 1:1 ratio of Δ8-mKate : ΔbslA-GFP, Δ8-mKate : Δeps(A-O)-GFP, Δ8-mKate : ΔtasA-GFP, or Δ8-

582 mKate : ΔbslA, Δeps(A-O),ΔtasA (ΔbΔeΔts) -GFP strains at day 3 (0.5% glutamic
583 acid (Ga) (w/v) and 1.5% milk (w/v); **C.** Biofilm stereoscope images of a 1:1 ratio of
584 Δ8-mKate : ΔbslA-GFP, Δ8-mKate : Δeps(A-O)-GFP, Δ8-mKate : ΔtasA-GFP, or Δ8-
585 mKate : ΔbslA, Δeps(A-O),ΔtasA (ΔbΔeΔts) -GFP strains at day 3 in 1% BSA (w/v);
586 **D.** and **F.** Quantification of the relative density of the GFP and mKate signal within
587 the biofilm footprint area for the conditions presented in **B.** and **C.** Each point
588 represents the relative density value (n=3) and the line represents the median value;
589 **E.** and **G.** Biofilm footprint area in cm^2 of NCIB 3610, Δ8 and for the conditions
590 presented in **B.** and **C.** Each point represents the footprint area value (n=5 biological
591 replicates) and the line represents the median value. T-test performed between
592 NCIB 3610 and Δ8 or coculture mixes: *** = p-value < 0.001. The raw intensity signal
593 for brightfield, GFP and mKate channels is shown in black and white and the merge
594 intensity signal of these two proteins is false coloured (green = GFP, magenta =
595 mKate). A representative image of three independent experiments is shown. The
596 scale bar represents 5 mm.

Discussion

Public goods are essential in microbial communities and are diverse in form and function (Momeni, 2018). Public goods are often produced by a subset of cells within the biofilm and the resultant materials are shared with other cells, even those not directly involved in production (Bachmann et al., 2013, Martin et al., 2020). This results in the potential for exploitation by non-producers. *B. subtilis* biofilms contain multiple public goods and, in this context, are typically thought of as the extracellular matrix molecules (Arnaouteli et al., 2021). The results presented here provide insight into the role of extracellular proteases, a newly defined biofilm public good, in the formation of *B. subtilis* colony biofilms. The extracellular proteases play an important role in biofilm formation, even when nitrogen is in the form of glutamic acid. These are nutrient conditions where growth under planktonic conditions is not impacted by their absence (Rosazza et al., 2023b), thereby showcasing the impact of different environmental conditions. Our experimental data suggest that the proteases support growth during colony biofilm development, potentially because their absence leads to restricted nutrient availability within the interior of the biofilm community, thus promoting sporulation. It is possible that materials released from dead cells in the biofilm (Asally et al., 2012) or from re-modelling / degradation of protein components in the matrix (Earl et al., 2020) are not accessible when these lytic enzymes are absent and therefore nutrients become limited in localised regions.

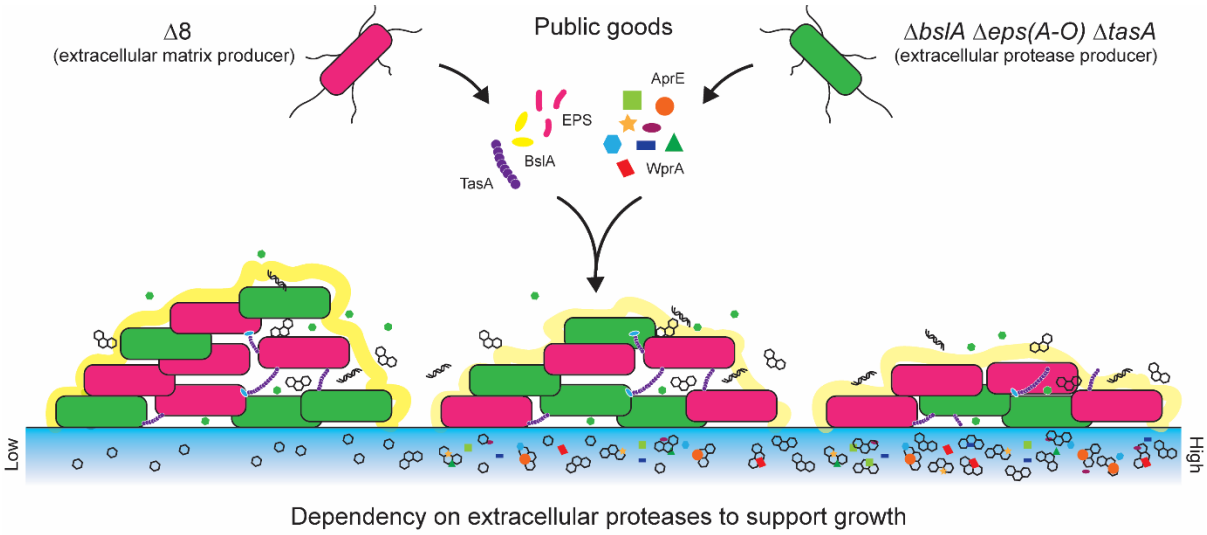

Figure 8 – Summary of the role of extracellular proteases and extracellular matrix proteins during biofilm formation in different ecological contexts Mixing extracellular matrix (Δ8) and extracellular proteases (Δ*bslA* Δ*eps(A-O)* Δ*tasA*) producer strains allow reciprocal sharing of these two classes of public goods in

biofilms. Increasing the dependency on extracellular proteases for growth impacts biofilm structure and coexistence of extracellular proteases and extracellular matrix proteins producers.

The role of individual extracellular proteases produced by *B. subtilis* in promoting biofilm formation was systematically investigated using a suite of single mutant and single producer strains derived from NCIB 3610. Interestingly, most single deletion strains did not significantly affect colony biofilm phenotype, with the architecture of the colony biofilms that formed mirroring the wild-type strain and with the findings for Vpr and NprE being consistent with previous work (Kobayashi and Ikemoto, 2019, Earl et al., 2020). However, the absence of AprE resulted in a distinct phenotype with smaller, scattered wrinkles, revealing a new role for AprE in colony biofilm formation. Furthermore, a WprA mono-producer strain (and to a lesser extend the Mpr monoproducer strain) exhibited a similar wrinkle phenotype to NCIB 3610, while other mono-producer strains resembled the Δ8 strain. These findings indicate that WprA is sufficient to allow wild-type-like biofilm architecture, albeit the targets are unknown and may include TasA. Collectively, these observations suggest that specific proteases have unique functions in biofilm formation, although for the most part, their target(s) remain undefined (Harwood and Kikuchi, 2022).

By modulating the nutrient source, we were able to influence both biofilm structure and hydrophobicity. The presence of polymeric nutrient sources increases the dependency on extracellular proteases for growth (Rosazza et al., 2023b). This dependency impacts biofilm formation, particularly under conditions where protease production becomes more costly (Rosazza et al., 2023b). The same is true in the case of biofilm formation. The findings highlight how the typical composition of the media used in a field of research can influence the experimental outcomes revealed and may even prevent important insights from being uncovered. Our data also showcase the adaptability of *B. subtilis* to varying nutrient sources and reveal the associated trade-offs in terms of protease production and biofilm structure.

We explored the concept of reciprocal sharing of extracellular proteases and matrix components in co-culture experiments and found that co-culturing the Δ8 strain with matrix mutant strains restores wild-type biofilm morphology, indicating that public good sharing can rescue biofilm structure. However, the relative cost of protease

655 production influences coexistence within these communities, as shown by
656 experiments where the dependency on the extracellular proteases for growth is
657 increased. *B. subtilis* produces other classes of extracellular enzymes, such as
658 lipases, and amylases (Eggert et al., 2003, Konsula and Liakopoulou-Kyriakides,
659 2004). Thus, it is highly likely that these groups of enzymes also serve as public
660 goods that become essential in specific growth contexts.

661 **Outlook**

662 Our findings provide valuable insights into the intricate interplay between
663 extracellular proteases and the biofilm matrix molecules in the context of public
664 goods and biofilm formation in *B. subtilis*. It also raises intriguing questions about the
665 specific functions of individual extracellular proteases and the ecological implications
666 of public goods sharing within biofilm communities. Understanding public goods
667 sharing in *B. subtilis* biofilms is not only relevant from a biological perspective, but
668 also has practical implications. Increased knowledge should provide insights into
669 biofilm resilience, the development of pro-biofilm strategies, and thus the potential for
670 engineering microbial communities for various applications.

Acknowledgements

Work was funded by the Biotechnology and Biological Science Research Council (BBSRC) [BB/P001335/1, BB/R012415/1]. TR was funded by Wellcome [102132/B/13/Z]. This research was funded in whole, or in part, by the Wellcome Trust [102132/B/13/Z]. CE was supported by the Wellcome Institutional Strategic Support Fund [Award no. 097818/Z/11]. The authors would like to thank Dr. Sofia Arnaouteli and Ms Tetyana Sukhodub for their support in generating some of the strains used in this study. The authors also thank Dr. Megan Bergkessel for her constructive discussions on this study. **For the purpose of open access, the author has applied a CC BY public copyright licence to any Author Accepted Manuscript version arising from this submission.**

Competing interests

The authors declare that they have no known competing financial interests or personal relationships that could have appeared to influence the work reported in this paper.

Data Availability Statement

Analysis code and experimental datasets have been deposited in the nrstanleywall GitHub repository (https://github.com/NSWlabDundee/) and archived by Zenodo (Rosazza et al., 2023a).

693 **Table 1 Strains used in this study**

Strain	Genotype[a]	Source/Construction [b]
NCIB 3610	Prototroph	*Bacillus* Genetic Stock Centre
NRS6017 (DK420)	NCIB 3610 *comI*^{Q12L}	(Konkol et al., 2013)
NRS5645	NCIB 3610 *comI*^{Q12L} *ΔaprE, Δbpr, Δepr, Δmpr, ΔnprB, ΔnprE, Δvpr, ΔwprA* (referred to as Δ8)	(Earl et al., 2019)
NRS1473	NCIB 3610 *sacA*-P*spachy-gfp* (*kan)*	(Verhamme et al., 2007)
NRS6556	NCIB 3610 *comI*^{Q12L} *amyE:: Phy-spank – mKate2 (cml)*	Gift from Professor Akos T. Kovacs
NRS3648	*Δ8 amyE:: Phy-spank-gfpmut2 (cml)*	pBL165 (Stanley et al., 2003)→ NRS5645
NRS3670	*Δ8 amyE:: Phy-spank-mKate2 (cml)*	pNW725 (Eigentler et al., 2021)→ NRS5645
NRS3657	NCIB 3610 *comI*^{Q12L} *ΔaprE::erm*	(Rosazza et al., 2023b)
NRS6047	NCIB 3610 *comI*^{Q12L} *Δbpr*	(Earl et al., 2019)
NRS3658	NCIB 3610 *comI*^{Q12L} *Δepr::erm*	(Rosazza et al., 2023b)
NRS3659	NCIB 3610 *comI*^{Q12L} *Δmpr::erm*	(Rosazza et al., 2023b)
NRS3660	NCIB 3610 *comI*^{Q12L} *ΔnprB::erm*	(Rosazza et al., 2023b)
NRS3661	NCIB 3610 *comI*^{Q12L} *ΔnprE::erm*	(Rosazza et al., 2023b)
NRS7010	NCIB 3610 *comI*^{Q12L} *Δvpr*	(Earl et al., 2019)
NRS6810	NCIB 3610 *comI*^{Q12L} *ΔwprA*	(Earl et al., 2019)
NRS3679	NCIB 3610 *comI*^{Q12L} Δ7 *aprE*^{WT} (*erm*)	(Rosazza et al., 2023b)
NRS3680	NCIB 3610 *comI*^{Q12L} Δ7 *bpr*^{WT} (*erm)*	(Rosazza et al., 2023b)
NRS3681	NCIB 3610 *comI*^{Q12L} Δ7 *epr*^{WT} *(erm)*	(Rosazza et al., 2023b)
NRS3682	NCIB 3610 *comI*^{Q12L} Δ7 *mpr*^{WT} *(erm)*	(Rosazza et al., 2023b)
NRS3683	NCIB 3610 *comI*^{Q12L} Δ7 *nprB*^{WT} *(erm)*	(Rosazza et al., 2023b)
NRS3684	NCIB 3610 *comI*^{Q12L} Δ7 *nprE*^{WT} *(erm)*	(Rosazza et al., 2023b)
NRS3885	NCIB 3610 *comI*^{Q12L} Δ7 *sacA::kan vpr*^{WT}	(Rosazza et al., 2023b)
NRS6362	NCIB 3610 *comI*^{Q12L} Δ7 *wprA*^{WT}	(Earl et al., 2019)
NRS3812	NCIB 3610 *comI*^{Q12L} *ΔbslA::(cml) sacA::Phy-spank-gfp mut2*	(Hobley et al., 2013)
NRS3798	NCIB 3610 *comI*^{Q12L} *Δeps(A-O)::tet amyE::Phy-spank-gfp mut2*	(Ostrowski et al., 2011)
NRS2984	NCIB 3610 *comI*^{Q12L} *ΔtasA::(spc) amyE::Phy-spank-gfp mut2*	(Ostrowski et al., 2011)

NRS6552	NCIB 3610 *comI*^{Q12L} *ΔbslA::(cml) Δeps(A-O)::tet ΔtasA::(spc) sacA::Phy-spank-gfp mut2*	(Earl et al., 2019)

694 [a.] Drug resistance cassettes are as follows: kan, kanamycin resistance; cml, chloramphenicol
695 resistance; spec, spectinomycin resistance; tetracycline resistance, tet; and erm,
696 erythromycin resistance.
697 [b.] Strain construction is denoted as DNA from donor strain transformed into recipient strain
698 following the direction of the arrow (→).

699

700 **Table 2 – Summary of the reciprocal sharing experiments**

	Growth Condition / Feature Assessed	Ga + Gly		Milk 1.5% + Gly		BSA 1% + Gly	
		NCIB 3610	Δ8	NCIB 3610	Δ8	NCIB 3610	Δ8
ΔbslA	WT-like structure:	YES	YES	YES	YES	YES	NO Non-wrinkled flat
	Coexistence:	YES	YES	YES	YES	NO NCIB 3610 wins	No Δ8 wins
	WT-like footprint:	YES	YES	YES	YES	NO >WT	YES
Δeps(A-O)	WT-like structure:	YES	YES	YES	YES	NO Non-wrinkled flat	NO Non-wrinkled flat
	Coexistence:	YES	YES	NO NCIB 3610 wins	NO Δ8 wins	NO *Δeps(A-O)* wins	NO *Δeps(A-O)* wins
	WT-like footprint:	YES	YES	YES	NO <WT	NO >WT	NO >WT
ΔtasA	WT-like structure:	YES	YES	YES	YES	NO Non-wrinkled flat	NO Non-wrinkled flat
	Coexistence:	YES	YES	YES	YES	NO NCIB 3610 wins	NO Δ8 wins
	WT-like footprint:	YES	YES	NO <WT	NO >WT	NO >WT	NO >WT
ΔbslA Δeps(A-O) ΔtasA	WT-like structure:	YES	YES	YES	YES	NO High spatial segregation	NO Large, flat community
	Coexistence:	YES	YES	YES	YES	NO mutant wins	NO Δ8 wins
	WT-like footprint:	YES	YES	NO <WT	NO >WT	NO <WT	NO >WT

701

702

References

ARMSTRONG, S. K. 2015. Bacterial Metabolism in the Host Environment: Pathogen Growth and Nutrient Assimilation in the Mammalian Upper Respiratory Tract. *Microbiol Spectr,* 3.

ARNAOUTELI, S., BAMFORD, N. C., STANLEY-WALL, N. R. & KOVACS, A. T. 2021. Bacillus subtilis biofilm formation and social interactions. *Nat Rev Microbiol,* 19**,** 600-614.

ARNAOUTELI, S., FERREIRA, A. S., SCHOR, M., MORRIS, R. J., BROMLEY, K. M., JO, J., CORTEZ, K. L., SUKHODUB, T., PRESCOTT, A. R., DIETRICH, L. E. P., MACPHEE, C. E. & STANLEY-WALL, N. R. 2017. Bifunctionality of a biofilm matrix protein controlled by redox state. *Proc Natl Acad Sci U S A,* 114**,** E6184-E6191.

ASALLY, M., KITTISOPIKUL, M., RUE, P., DU, Y., HU, Z., CAGATAY, T., ROBINSON, A. B., LU, H., GARCIA-OJALVO, J. & SUEL, G. M. 2012. Localized cell death focuses mechanical forces during 3D patterning in a biofilm. *Proc Natl Acad Sci U S A,* 109**,** 18891-6.

BACHMANN, H., FISCHLECHNER, M., RABBERS, I., BARFA, N., BRANCO DOS SANTOS, F., MOLENAAR, D. & TEUSINK, B. 2013. Availability of public goods shapes the evolution of competing metabolic strategies. *Proc Natl Acad Sci U S A,* 110**,** 14302-7.

BRANDA, S. S., CHU, F., KEARNS, D. B., LOSICK, R. & KOLTER, R. 2006. A major protein component of the Bacillus subtilis biofilm matrix. *Mol Microbiol,* 59**,** 1229-38.

BRANDA, S. S., GONZALEZ-PASTOR, J. E., BEN-YEHUDA, S., LOSICK, R. & KOLTER, R. 2001. Fruiting body formation by Bacillus subtilis. *Proc Natl Acad Sci U S A,* 98**,** 11621-6.

CEZAIRLIYAN, B. & AUSUBEL, F. M. 2017. Investment in secreted enzymes during nutrient-limited growth is utility dependent. *Proc Natl Acad Sci U S A,* 114**,** E7796-E7802.

DRAGOS, A., KIESEWALTER, H., MARTIN, M., HSU, C. Y., HARTMANN, R., WECHSLER, T., ERIKSEN, C., BRIX, S., DRESCHER, K., STANLEY-WALL, N., KUMMERLI, R. & KOVACS, A. T. 2018. Division of Labor during Biofilm Matrix Production. *Curr Biol,* 28**,** 1903-1913 e5.

DRESCHER, K., NADELL, C. D., STONE, H. A., WINGREEN, N. S. & BASSLER, B. L. 2014. Solutions to the public goods dilemma in bacterial biofilms. *Curr Biol,* 24**,** 50-55.

EARL, C., ARNAOUTELI, S., BAMFORD, N. C., PORTER, M., SUKHODUB, T., MACPHEE, C. E. & STANLEY-WALL, N. R. 2020. The majority of the matrix protein TapA is dispensable for Bacillus subtilis colony biofilm architecture. *Mol Microbiol,* 114**,** 920-933.

EARL, C., ARNAOUTELI, S., SUKHODUB, T., MACPHEE, C. E. & STANLEY-WALL, N. R. 2019. The majority of the matrix protein TapA is dispensable for biofilm formation by Bacillus subtilis. *bioRxiv***,** 794164.

EGGERT, T., BROCKMEIER, U., DRÖGE, M. J., QUAX, W. J. & JAEGER, K. E. 2003. Extracellular lipases from Bacillus subtilis: regulation of gene expression and enzyme activity by amino acid supply and external pH. *FEMS Microbiol Lett,* 225**,** 319-24.

EIGENTLER, L., KALAMARA, M., BALL, G., MACPHEE, C. E., STANLEY-WALL, N. R. & DAVIDSON, F. A. 2021. Founder cell configuration drives competitive outcome within colony biofilms. *bioRxiv***,** 2021.07.08.451560.

ERRINGTON, J. 1993. Bacillus subtilis sporulation: regulation of gene expression and control of morphogenesis. *Microbiol Rev,* 57**,** 1-33.

FEI, C., MAO, S., YAN, J., ALERT, R., STONE, H. A., BASSLER, B. L., WINGREEN, N. S. & KOSMRLJ, A. 2020. Nonuniform growth and surface friction determine bacterial biofilm morphology on soft substrates. *Proc Natl Acad Sci U S A,* 117**,** 7622-7632.

FLEMMING, H. C., NEU, T. R. & WOZNIAK, D. J. 2007. The EPS matrix: the "house of biofilm cells". *J Bacteriol,* 189**,** 7945-7.

FLEMMING, H. C. & WINGENDER, J. 2010. The biofilm matrix. *Nat Rev Microbiol,* 8**,** 623-33.

FLEMMING, H. C., WINGENDER, J., SZEWZYK, U., STEINBERG, P., RICE, S. A. & KJELLEBERG, S. 2016. Biofilms: an emergent form of bacterial life. *Nat Rev Microbiol,* 14**,** 563-75.

HAMID, R., KHAN, M. A., AHMAD, M., AHMAD, M. M., ABDIN, M. Z., MUSARRAT, J. & JAVED, S. 2013. Chitinases: An update. *J Pharm Bioallied Sci,* 5**,** 21-9.

HARDER, W. & DIJKHUIZEN, L. 1983. Physiological responses to nutrient limitation. *Annu Rev Microbiol,* 37**,** 1-23.

HARWOOD, C. R. & KIKUCHI, Y. 2022. The ins and outs of Bacillus proteases: activities, functions and commercial significance. *FEMS Microbiol Rev,* 46.

HIBBING, M. E., FUQUA, C., PARSEK, M. R. & PETERSON, S. B. 2010. Bacterial competition: surviving and thriving in the microbial jungle. *Nat Rev Microbiol,* 8**,** 15-25.

HILL, B. H., MCCORMICK, F. H., HARVEY, B. C., JOHNSON, S. L., WARREN, M. L. & ELONEN, C. M. 2010. Microbial enzyme activity, nutrient uptake and nutrient limitation in forested streams. *Freshwater Biology,* 55**,** 1005-1019.

HOBLEY, L., OSTROWSKI, A., RAO, F. V., BROMLEY, K. M., PORTER, M., PRESCOTT, A. R., MACPHEE, C. E., VAN AALTEN, D. M. & STANLEY-WALL, N. R. 2013. BslA is a self-assembling bacterial hydrophobin that coats the Bacillus subtilis biofilm. *Proc Natl Acad Sci U S A,* 110**,** 13600-5.

HUNTER, J. D. 2007. Matplotlib: A 2D Graphics Environment. *Computing in Science & Engineering,* 9**,** 90-95.

KALAMARA, M., ABBOTT, J. C., MACPHEE, C. E. & STANLEY-WALL, N. R. 2021. Biofilm hydrophobicity in environmental isolates of Bacillus subtilis. *bioRxiv***,** 2021.04.29.441976.

KEARNS, D. B. 2008. Division of labour during Bacillus subtilis biofilm formation. *Mol Microbiol,* 67**,** 229-31.

KJELDGAARD, B., LISTIAN, S. A., RAMASWAMHI, V., RICHTER, A., KIESEWALTER, H. T. & KOVACS, A. T. 2019. Fungal hyphae colonization by Bacillus subtilis relies on biofilm matrix components. *Biofilm,* 1**,** 100007.

KLUYVER, T., RAGAN-KELLEY, B., PEREZ, F., GRANGER, B., BUSSONNIER, M., FREDERIC, J., KELLEY, K., HAMRICK, J., GROUT, J., CORLAY, S., IVANOV, P., AVILA, D., ABDALL, S. & WILLING, C. 2016. Jupyter Notebooks -- a publishing format for reproducible computational workflows. *IOS Press***,** 87 - 90.

KOBAYASHI, K. 2007. Gradual activation of the response regulator DegU controls serial expression of genes for flagellum formation and biofilm formation in Bacillus subtilis. *Mol Microbiol,* 66**,** 395-409.

KOBAYASHI, K. & IKEMOTO, Y. 2019. Biofilm-associated toxin and extracellular protease cooperatively suppress competitors in Bacillus subtilis biofilms. *PLoS Genet,* 15**,** e1008232.

KOBAYASHI, K. & IWANO, M. 2012. BslA(YuaB) forms a hydrophobic layer on the surface of Bacillus subtilis biofilms. *Mol Microbiol,* 85**,** 51-66.

KONKOL, M. A., BLAIR, K. M. & KEARNS, D. B. 2013. Plasmid-encoded ComI inhibits competence in the ancestral 3610 strain of Bacillus subtilis. *J Bacteriol,* 195**,** 4085-93.

KONSULA, Z. & LIAKOPOULOU-KYRIAKIDES, M. 2004. Hydrolysis of starches by the action of an α-amylase from Bacillus subtilis. *Process Biochemistry,* 39**,** 1745-1749.

LOPEZ, D., VLAMAKIS, H. & KOLTER, R. 2010. Biofilms. *Cold Spring Harb Perspect Biol,* 2**,** a000398.

LORENSEN, W. E. & CLINE, H. E. 1987. Marching cubes: A high resolution 3D surface construction algorithm. *Proceedings of the 14th annual conference on Computer graphics and interactive techniques.* Association for Computing Machinery.

MAHAPATRA, S., YADAV, R. & RAMAKRISHNA, W. 2022. Bacillus subtilis impact on plant growth, soil health and environment: Dr. Jekyll and Mr. Hyde. *J Appl Microbiol,* 132**,** 3543-3562.

MAHMOOD, F., KASHIF UR REHMAN, S., JAMEEL, M., RIAZ, N., JAVED, M. F., SALMI, A. & AWAD, Y. A. 2022. Self-Healing Bio-Concrete Using Bacillus subtilis Encapsulated in Iron Oxide Nanoparticles. *Materials (Basel),* 15.

MARLOW, V. L., CIANFANELLI, F. R., PORTER, M., CAIRNS, L. S., DALE, J. K. & STANLEY-WALL, N. R. 2014. The prevalence and origin of exoprotease-producing cells in the Bacillus subtilis biofilm. *Microbiology,* 160**,** 56-66.

MARTIN, M., DRAGOS, A., OTTO, S. B., SCHAFER, D., BRIX, S., MAROTI, G. & KOVACS, A. T. 2020. Cheaters shape the evolution of phenotypic heterogeneity in Bacillus subtilis biofilms. *ISME J,* 14**,** 2302-2312.

MERINO, N., ARONSON, H. S., BOJANOVA, D. P., FEYHL-BUSKA, J., WONG, M. L., ZHANG, S. & GIOVANNELLI, D. 2019. Corrigendum: Living at the Extremes: Extremophiles and the Limits of Life in a Planetary Context. *Frontiers in Microbiology,* 10.

MOMENI, B. 2018. Division of Labor: How Microbes Split Their Responsibility. *Curr Biol,* 28**,** R697-R699.

MORRIS, R. J., STEVENSON, D., SUKHODUB, T., STANLEY-WALL, N. R. & MACPHEE, C. E. 2022. Density and temperature controlled fluid extraction in a bacterial biofilm is determined by poly-γ-glutamic acid production. *NPJ Biofilms Microbiomes,* 8**,** 98.

OREN, A. 2008. Microbial life at high salt concentrations: phylogenetic and metabolic diversity. *Saline Systems,* 4**,** 2.

OSTROWSKI, A., MEHERT, A., PRESCOTT, A., KILEY, T. B. & STANLEY-WALL, N. R. 2011. YuaB functions synergistically with the exopolysaccharide and TasA amyloid fibers to allow biofilm formation by Bacillus subtilis. *J Bacteriol,* 193**,** 4821-31.

ROSAZZA, T., EARL, C., EIGENTLER, L., DAVIDSON, F. & STANLEY-WALL, N. 2023a. Code for Rosazza et al. 2023 Reciprocal sharing of two classes of public goods facilitates Bacillus subtilis biofilm formation (v1.0). *Zenodo*.

ROSAZZA, T., EIGENTLER, L., EARL, C., DAVIDSON, F. A. & STANLEY-WALL, N. R. 2023b. Bacillus subtilis extracellular protease production incurs a context-dependent cost. *Mol Microbiol,* 120**,** 105-121.

SCHONBICHLER, A., DIAZ-MORENO, S. M., SRIVASTAVA, V. & MCKEE, L. S. 2020. Exploring the Potential for Fungal Antagonism and Cell Wall Attack by Bacillus subtilis natto. *Front Microbiol,* 11**,** 521.

STANLEY, N. R., BRITTON, R. A., GROSSMAN, A. D. & LAZAZZERA, B. A. 2003. Identification of catabolite repression as a physiological regulator of biofilm formation by Bacillus subtilis by use of DNA microarrays. *J Bacteriol,* 185**,** 1951-7.

TRIUNFO, M., TAFI, E., GUARNIERI, A., SALVIA, R., SCIEUZO, C., HAHN, T., ZIBEK, S., GAGLIARDINI, A., PANARIELLO, L., COLTELLI, M. B., DE BONIS, A. & FALABELLA, P. 2022. Characterization of chitin and chitosan derived from Hermetia illucens, a further step in a circular economy process. *Sci Rep,* 12**,** 6613.

VAN DER WALT, S., SCHONBERGER, J. L., NUNEZ-IGLESIAS, J., BOULOGNE, F., WARNER, J. D., YAGER, N., GOUILLART, E., YU, T. & SCIKIT-IMAGE, C. 2014. scikit-image: image processing in Python. *PeerJ,* 2**,** e453.

VERHAMME, D. T., KILEY, T. B. & STANLEY-WALL, N. R. 2007. DegU co-ordinates multicellular behaviour exhibited by Bacillus subtilis. *Mol Microbiol,* 65**,** 554-68.

VLAMAKIS, H., AGUILAR, C., LOSICK, R. & KOLTER, R. 2008. Control of cell fate by the formation of an architecturally complex bacterial community. *Genes Dev,* 22**,** 945-53.

WASKOM, M. L. 2021. seaborn: statistical data visualization. *Journal of Open Source Software,* 6**,** 3021.

WEST, S. A. & COOPER, G. A. 2016. Division of labour in microorganisms: an evolutionary perspective. *Nat Rev Microbiol,* 14**,** 716-723.

Supplemental Material

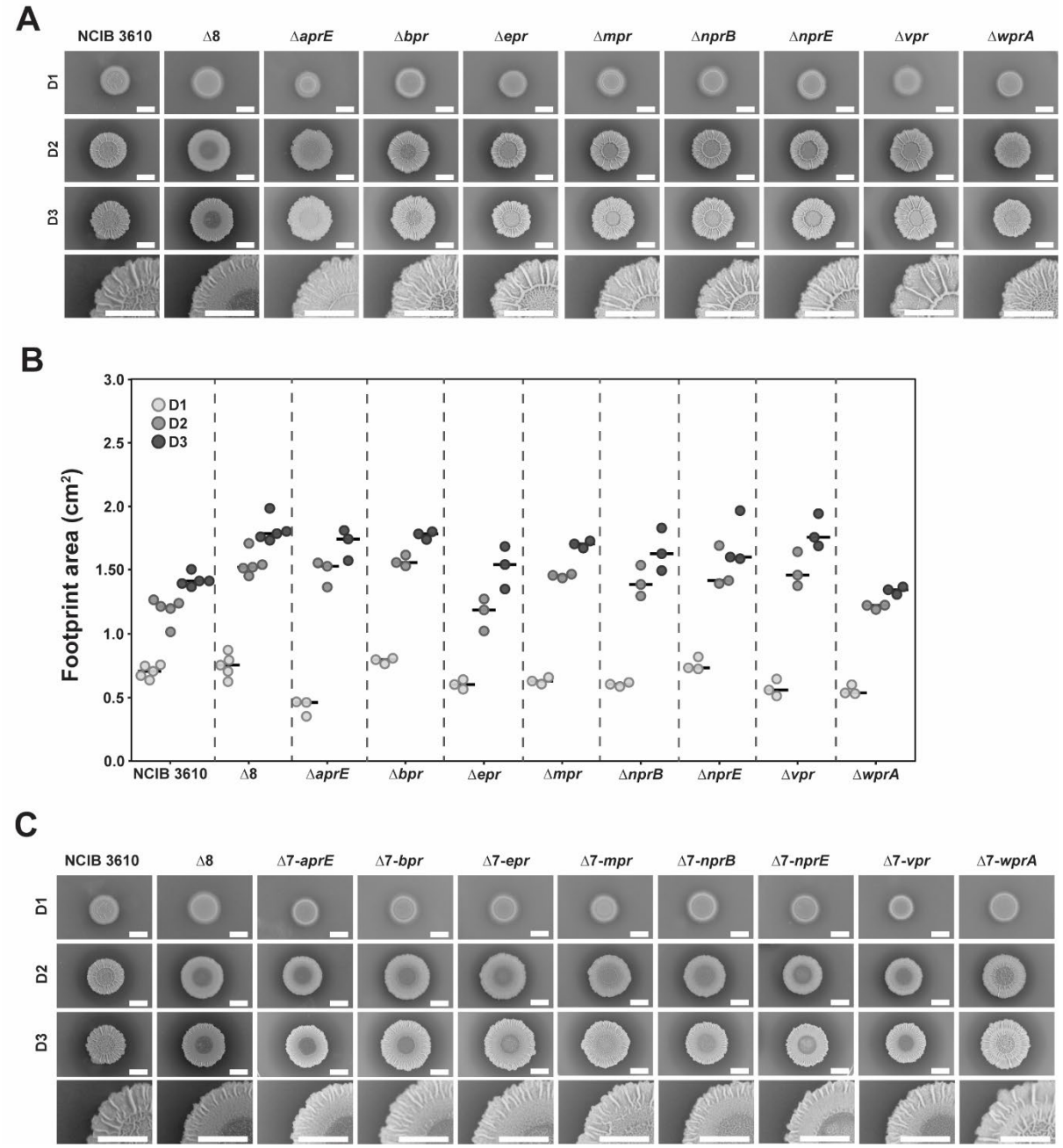

Figure S1 – Single deletion and monoproducers strains exhibit different biofilm phenotypes A. Biofilm reflected light images of NCIB 3610, Δ8 and single deletion strains over time (day 1 to day 3). A zoom of the day 3 image is in the bottom row. The scale bar represents 5 mm; **B.** Biofilm footprint area in cm^2 of NCIB 3610, Δ8 and single deletion strains over time (day 1 to day 3) in. Each point represents the footprint area value (n=5 biological replicates for NCIB 3610 and Δ8 and n=3 for single deletion strains) and the line represents the median value. **C.** Biofilm reflected light images of NCIB 3610, Δ8 and monoproducer strains over time (day 1 to day 3). The scale bar represents 5 mm.

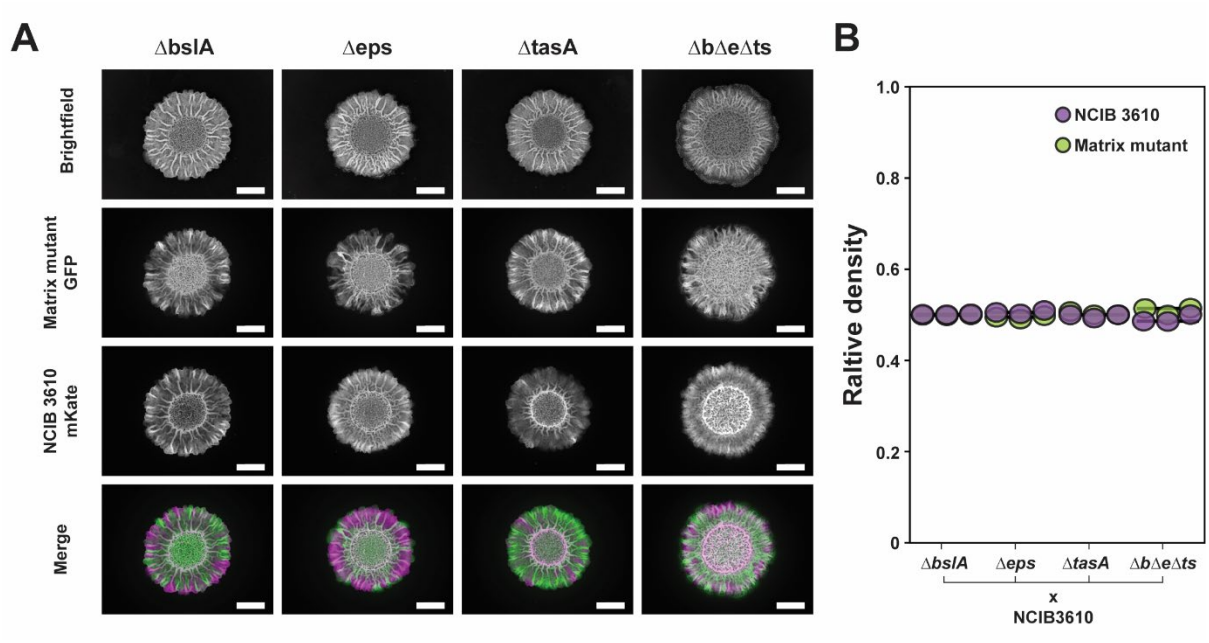

Figure S2 – NCIB 3610 and extracellular matrix component producers coexist on a non-polymeric nutrient source. A. Biofilm stereoscope images of a 1:1 ratio of NCIB 3610-mKate : ΔbslA-GFP, NCIB 3610-mKate : Δeps(A-O)-GFP, NCIB 3610-mKate : ΔtasA-GFP, or NCIB 3610-mKate : ΔbslA, Δeps(A-O),ΔtasA (ΔbΔeΔts) - GFP strains at day 3 in 0.5% glutamic acid (w/v), 0.5% glycerol (v/v), 1.5% (w/v) agar (Ga+Gly). The raw intensity signal for brightfield, GFP and mKate proteins is shown in black and white and the merge intensity signal of these two proteins is shown in colour (green = GFP, magenta = mKate). A representative image of three independent experiments is shown. The scale bar represents 5 mm; **B.** Quantification of the relative density of the GFP and mKate signal within the biofilm footprint area for the conditions presented in A. Each point represents the relative density value (n=3) and the line represents the median value.

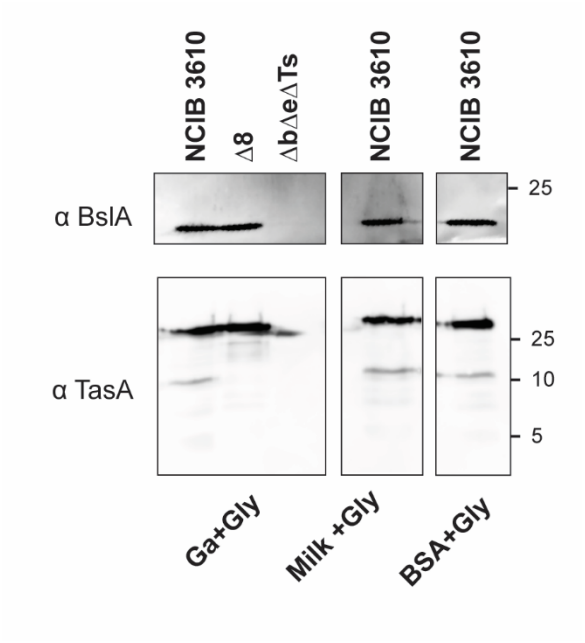

Figure S3 – Extracellular matrix proteins are produced in when nutrients are polymeric. Images of immunoblot against BslA (top image) and TasA (bottom image) on biofilm protein extract obtained after 3 days from NCIB 3610, Δ8 and the ΔbslA, Δeps(A-O), ΔtasA (ΔbΔeΔts) strains. A representative image of three independent experiments is shown (left part of the image correspond to Figure 3).

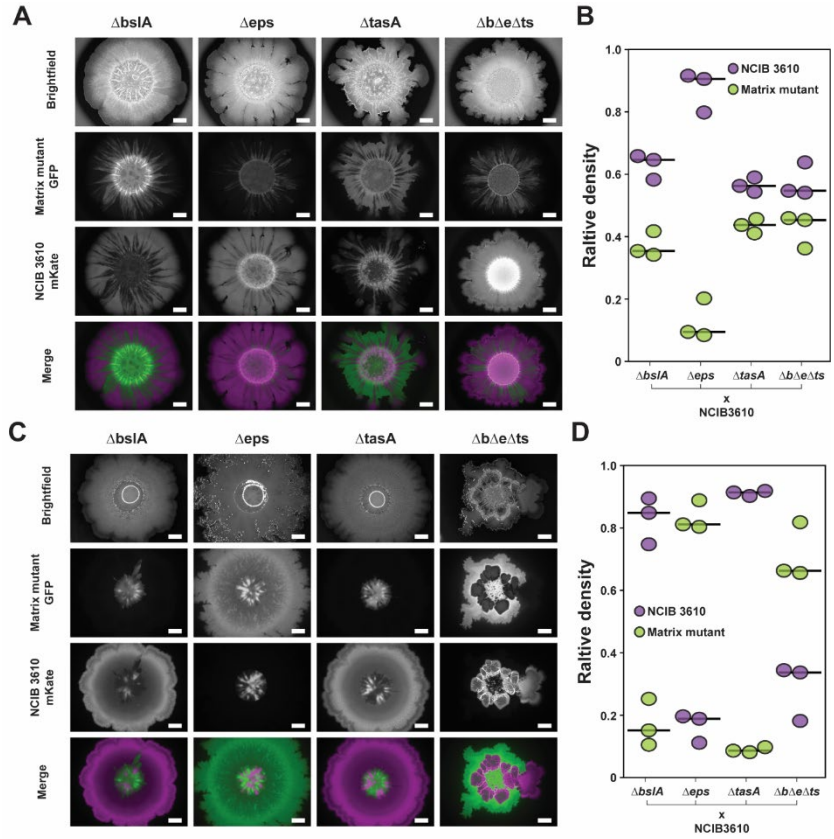

Figure S4 – NCIB 3610 and extracellular matrix component producers engaged differentially in the division of labour in the presence of polymeric nutrient sources A. Biofilm stereoscope images of a 1:1 ratio of NCIB 3610-mKate : ΔbslA-GFP, NCIB 3610-mKate : Δeps(A-O)-GFP, NCIB 3610-mKate : ΔtasA-GFP, or NCIB 3610-mKate : ΔbslA, Δeps(A-O),ΔtasA (ΔbΔeΔts) -GFP strains at day 3 in 1.5% milk (w/v), 0.5% glycerol (v/v), 1.5% (w/v) agar (milk+Gly) The raw intensity signal for brightfield, GFP and mKate proteins is shown in black and white and the merge intensity signal of these two proteins is shown in colour (green = GFP, magenta = mKate). A representative image of three independent experiments is shown. The scale bar represents 5 mm; **B.** Quantification of the relative density of the GFP and mKate signal within the biofilm footprint area for the conditions presented in A. Each point represents the relative density value (n=3) and the line represents the median value; **C.** Biofilm stereoscope images of a 1:1 ratio of NCIB 3610-mKate : ΔbslA-GFP, NCIB 3610-mKate : Δeps(A-O)-GFP, NCIB 3610-mKate : ΔtasA-GFP, or NCIB 3610-mKate : ΔbslA, Δeps(A-O),ΔtasA (ΔbΔeΔts) -GFP strains at day 3 in 1% BSA (w/v), 0.5% glycerol (v/v), 1.5% (w/v) agar (BSA+Gly) The raw intensity signal for brightfield, GFP and mKate proteins is shown in black and white and the merge intensity signal of these two proteins is shown in colour (green = GFP, magenta = mKate). A representative image of three independent experiments is shown. The scale bar represents 5 mm; **D.** Quantification of the relative density of the GFP and mKate signal within the biofilm footprint area for the conditions presented in C. Each point represents the relative density value (n=3) and the line represents the median value.